Synthesis and Characterization of

Ti_3SiC_2/Mg and Cr_2AlC/Mg Composites

A Thesis

Submitted to the Faculty

of

Drexel University

By

Matthew Jared Nelson

in partial fulfillment of the

requirements for the degree

of

Master of Science in Materials Science and Engineering

June 2014

Acknowledgements

First and foremost I want to acknowledge my mother, aunt, uncle and step-mother for always believing in me and knowing that I was destined to achieve more. Without their unwavering patience, love and support, none of this may have been possible.

I want to share my appreciation for Dr. Michel Barsoum and his grace for offering me such a wonderful opportunity to work in his group and offering support in so many different ways.

I feel it's important to acknowledge Dr. Babak Anasori and Darin Tallman for their extensive training and help on so many conceptual challenges for the successful completion of this work. Without hesitation, they were always willing to help and I owe them a great deal of thanks.

Through my time and experience with the MAX phase group I have gained some of the best friends I have in my life and consider Dr. Barsoum a treasured friend and confidant.

Lastly, this work would not have been possible without the funding coming from the United States Army Research Office; Hoorah.

To family, friends and a life full of love, peace and happiness – cheers.

Table of Contents

LIST OF TABLES

LIST OF FIGURES

Abstract

Synthesis and Characterization of the Mechanical Properties of
Ti_3SiC_2/Mg and Cr_2AlC/Mg Alloy Composites
Matthew Jared Nelson
Dr. Michel Barsoum, Ph.D.

High strength, light-weight materials are in high demand in many applications; especially aerospace and the military. The focus of this work is to report on the fabrication and characterization of Ti_3SiC_2 and Cr_2AlC MAX phase reinforced Mg and Mg-alloy metal matrix composites synthesized by pressureless melt infiltration. Pure Mg and Al-containing Mg-alloys (AZ31, AZ61 & AZ91) with varying Al content were matrices with loadings of ~ 45 ± 1 vol. %. The resulting microstructures and mechanical properties were characterized by X-ray diffraction, scanning electron microscopy (SEM), and compressive stress testing. SEM revealed kinked, delaminated, and elongated Ti_3SiC_2 grain, and non-deformed, rounded Cr_2AlC grain morphologies. Like in the Ti_2AlC/Mg composite system, increasing the Al wt. % content in the matrix enhanced the mechanical properties of the Ti_3SiC_2 composite system, but had a deleterious effect on the properties of the Cr_2AlC composite system. At 1.9 ± 0.1 GPa, 346 ± 4 MPa and 617 ± 10 MPa, the Vickers hardness, yield strength and ultimate compressive strength, respectively, of the Ti_3SiC_2/AZ91 composite were the highest in this study. All composites fabricated in this work exhibited fully and spontaneously reversible hysteresis loops due to the back and forth motion of dislocations. A small change in reinforcement volume fraction was found to affect the measured mechanical properties.

1. Introduction

Society's expectations and demands for newer and better technology have never been stronger than now. Society as a whole has become accustomed to having innovative new products introduced continuously. Recognizably, many industries would be more profitable and society would benefit from having stronger, lighter and cheaper materials. From aerospace and automotive, to nuclear and military applications, the demand is growing ever stronger for more innovative products consisting of materials that will perform longer, provide a safer and more reliable experience and have better performance overall. A major problem is that society, the military and various industries are demanding the realization and creation of the next era of elite materials now.

The United States military is very interested in advanced materials such as hybrid composites, metal matrix and ceramic matrix composites (MMCs and CMCs), and polymer matrix composites. One concept is to plate a vehicle, or tank, in advanced armor that is 1/3 the thickness, and 2/3 the weight, offering the same or better protection of typical armor. Armor such as this provides a protection benefit and increases the odds that military troops are brought home from battle safely. Reduced weight also enables vehicles to expend less energy to travel the same distance, making them more efficient; this is a highly revered quality for military vehicles.

Engineered armor, such as Dragon Skin made by Pinnacle Armor of Fresno, California is comprised of advanced ceramic and titanium carbide ultra-light, linked,

small discs. Dragon Skin provides increased dexterity and mobility instead of large heavy plates, or cumbersome vests, that restrict movement on infantry units.[1] The armor combines highly desirable characteristics: it is light weight with a high degree of vibrational damping and is extremely tough. The armor has the ability to resist multiple shots from steel-core shelled armor piecing rounds that can tear through quarter inch steel plate with ease. Quarter inch steel plate is typically found on lightly armored vehicles therefore, a dexterous, lightweight armor system which can protect soldiers from armor piercing bullets is very desirable.

Globally, militaries are interested in advanced materials which offer the next level of elite armor for soldier and vehicle protection. The military is not the only entity that is interested in upper echelon materials. The aerospace and automotive industries invest heavily in research and development for lighter, stronger materials that have a direct impact on energy consumption. In the aerospace industry, lighter weights correspond to enormous savings in fuel costs. Airline manufacturers would willingly spend extra money on materials to further improve cost-to-benefit ratios. Fuel savings could be kicked-back to the consumer in the form of cheaper flights which would equate to increased ticket sales and higher profitability. Having these benefits is strongly favored especially with the increasing costs and steady depletion of non-renewable fuels. The automotive industry can benefit in the same way. This is especially true in the racing sector where lighter cars equate to faster lap times and faster lap times increase the odds of winning large sums of money and prestige.

2. Background

2.1 Magnesium

Magnesium is the sixth most abundant element representing 2.7% of the total earth's crust and it is the third most abundant dissolved mineral in seawater at 1.1 kgm^{-3} .[2] Mg is not readily found in its elemental form; Mg is extracted from compounds such as magnesite ($MgCO_3$), dolomite ($MgCO_3$-$CaCO_3$), carnalite (KCl-$MgCl_2$-$6H_2O$), and also seawater.[2] Magnesium is the lightest of all structural materials, with a density of 1.74 gcm^{-3} making it 1/4 the density of steel and 2/3 the density of aluminum.[2]

Mg has good castability, can be milled at high speed, can be welded under controlled atmosphere and has improved damping ability in comparison to Al.[3,4] Despite some of its very desirable properties, Mg is not used for structural applications when compared to other engineered materials because of its low elastic modulus, low strengths (Fig. 1), creep resistance at elevated temperatures, and high chemical reactivity.[3]

Pure Magnesium	Annealed Sheet	Hand-Rolled Sheet	Sand Cast	Extruded	PM-Extruded	DMD-Extruded
0.2% Compressive yield strength (MPa)	69–83	105–115	21	34–55	92 ± 12^a	74 ± 4^b
0.2% Tensile yield strength (MPa)	90–105	115–140	21	69–105	132 ± 7^c	97 ± 2^d
Ultimate tensile strength (MPa)	160–195	180–220	90	165–205	193 ± 2^c	173 ± 1^d
Hardness HB[e]	40–41	45–47	30	35	—	—

Figure 1: Mechanical properties of pure Mg from various processing techniques.[2]

Interestingly, in comparisons with mechanical properties of medical implants, magnesium has a lower density, greater fracture toughness than hydroxyapatite, and its elastic modulus and yield strength are comparable to that of natural bone (Fig. 2).

Materials	Density (g/cm^3)	Fracture Toughness (MPa $m^{1/2}$)	Elastic Modulus (GPa)	Compressive Yield Strength (MPa)
Natural bone	1.8–2.1	3–6	3–20	130–180
Ti alloy	4.4–4.5	55–115	110–117	758–1117
Co–Cr alloy	8.3–9.2	—	230	450–1000
Stainless steel	7.9–8.1	50–200	189–205	170–310
Magnesium	1.74–2.0	15–40	41–45	65–100
Hydroxyapatite	3.1	0.7	73–117	600

Figure 2: Comparison of mechanical properties of medical implant materials to that of human bone and magnesium.[2]

2.2 Magnesium Alloys

Magnesium and its alloys have been used in a wide variety of applications ranging from automotive racing, spacecraft and missiles, medical devices and electronics, sports equipment, and more. Due to their lightweight, high specific properties (Figs. 3-4), and excellent machinability and damping capability, Mg-alloys have been widely used in aerospace, automotive, and the electronics industry for decades. [3,5,6]

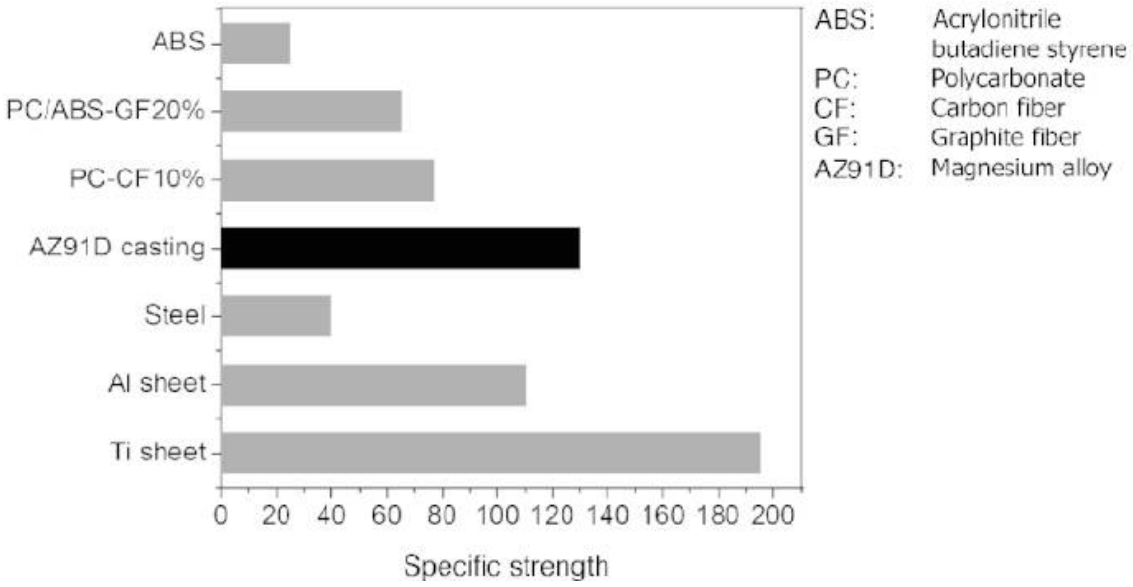

Figure 3: Specific strengths of structural materials in comparison with casted Mg-alloy AZ91D.[2]

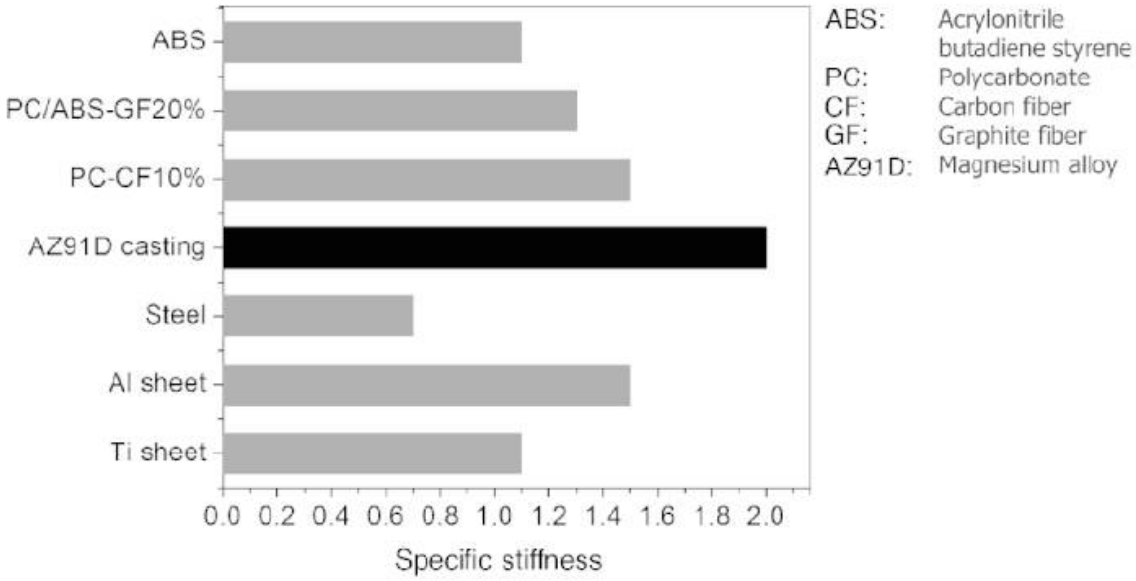

Figure 4: Specific stiffness of structural materials in comparison with casted Mg-alloy AZ91D.[2]

In the 1920's Mg parts had been integrated into racing cars. In the subsequent decade, over 20 kg of Mg-alloy was used for the transmission housing and crankcase of the VW Beetle.[2] Since the realization of their benefits, various Mg automotive components have been incorporated in vehicles (Fig. 5).

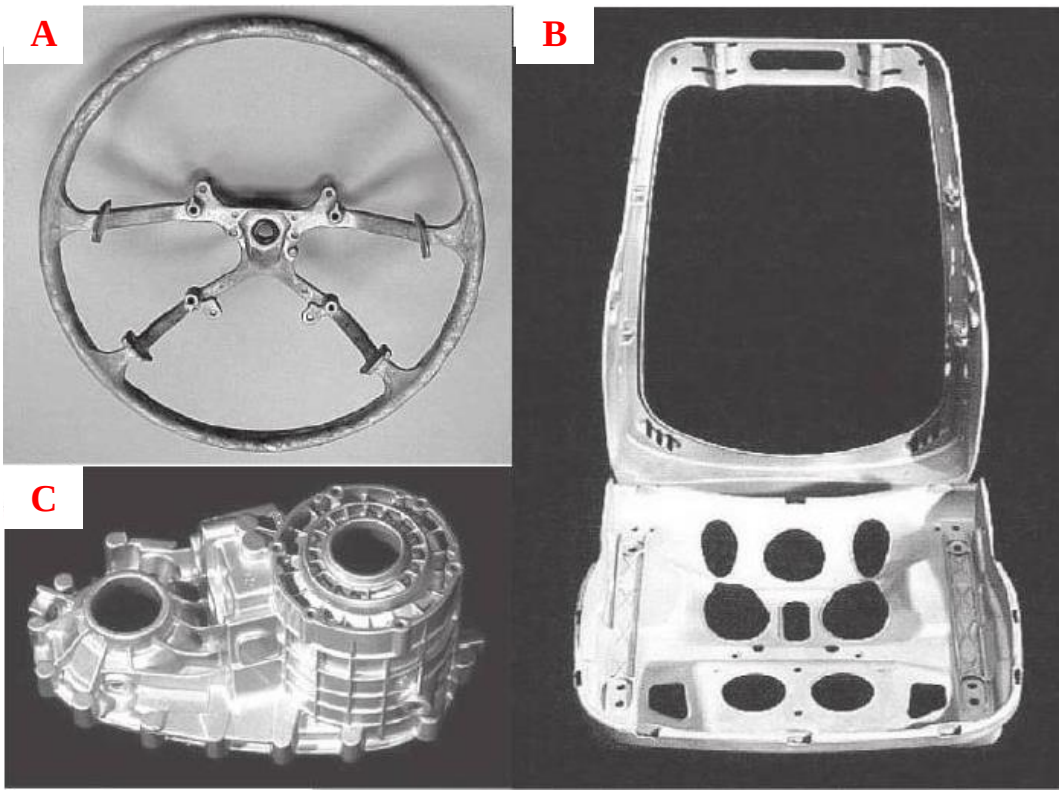

Figure 5: Toyota Camry steering wheel core: 0.75 kg (A); Jaguar and Fiat model seat support: 2.6 kg (B); AZ91D rear transfer case: 2.7 kg (C).[2]

In the past decade, increasing environmental, legislative and global concerns have pressured manufacturers, especially automotive and aerospace, to produce higher fuel efficiency, lighter and higher performance vehicles. This has spurred a major surge in the harvesting and usage of Mg.[2]

Fiber metal laminates, aluminum, and low-density structural plastics have been introduced and used over the years in aerospace component development in attempts to reduce weight and therefore reduce operational costs.[2] Metal laminate cost-to-benefit ratios, challenges preventing aluminum alloys having further weight reduction and the

poor impact, damage tolerance and temperature resistance of low-density structural plastics have made Mg-alloys an attractive weight reduction material.[2]

Mg-based materials have been used in both civil and military aircraft. Civil applications include thrust reversers for the Boeing 737, 747, 757, and 767. Rolls-Royce has used them in gearboxes, engines and helicopter transmission casings. Mg-alloys have been also been used for Eurofighter Typhoon, Tornado and F16 military aircraft transmission casings.[2]

Mg-alloy usage becomes especially significant for spacecraft and missiles where lift-off weight requirements are strict and vibrational damping capability becomes extremely beneficial. Large amounts of magnesium where used in intercontinental ballistic missiles. Besides their reduced weight and damping properties, Mg-alloys are attractive for space applications because of their high specific properties, elevated temperature resistance, ease of fabrication, and their resilience to other issues such as ozone, high energy particle and small meteorite bombardment.[2]

Included in the popularity of their usage across various industries, Mg-alloys have also received wide exposure in research activity. Spanning the years from 1990 to 2007 Mg-alloys AZ31 and AZ91 have appeared, with an exponential presence, in hundreds of scientific articles world-wide (Fig. 6).

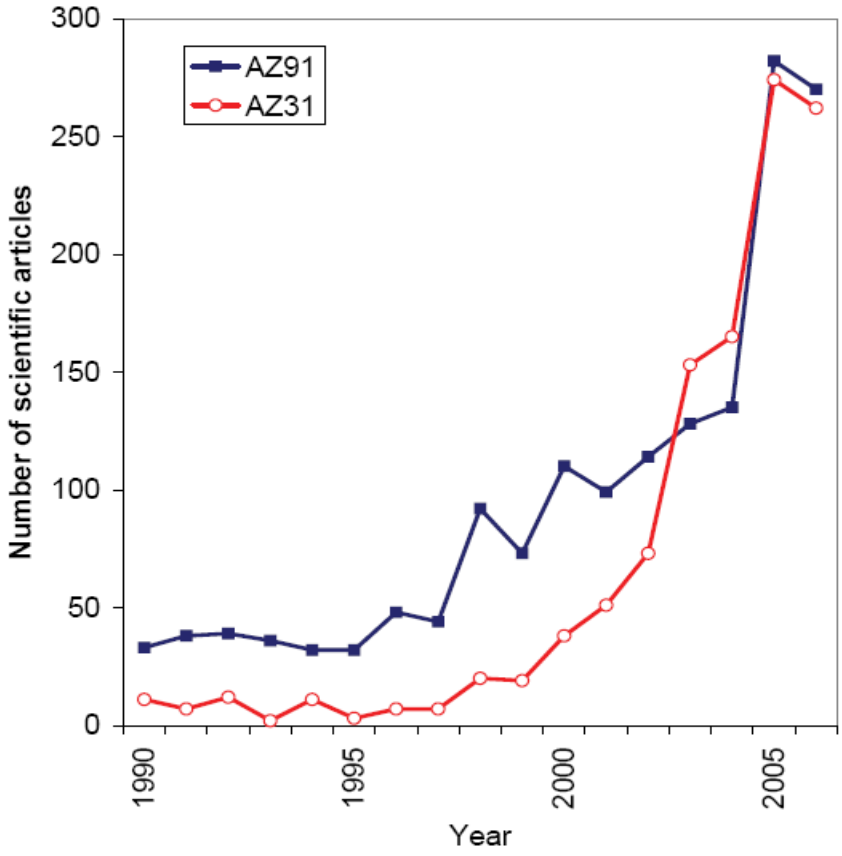

Figure 6: Number of scientific articles which have terms AZ91 or AZ31 in the abstract.[7]

2.3 Metal Matrix Composites

Developmental efforts on MMCs in the 1950s and early 1960s were driven by the need to find materials that would dramatically extend structural efficiency of metallic materials while retaining their advantages: chemical inertness, high shear strength, and good property retention at high temperatures.[8] Early work on sintered aluminum powder was a precursor to discontinuously reinforced MMCs. Subsequent development of high-strength monofilaments, first boron and then silicon carbide (SiC), enabled MMC

advancement throughout the 1960s and early 1970s.[8] In the late 1960's research on MMCs was due to the high performance needs of the aerospace industry.[9]

Historically, steel-wire reinforced copper fibers were one of the first continuous-fiber reinforced composites. These composites were used to study MMCs as a model system[9]. It was during this time that performance was the main focus and cost was not the primary concern. Soon after, boron filaments were used as the first high-strength, high-modulus reinforcement that was developed for both MMC and organic matrix composites (OMC).[9] Processing issues associated with fiber damage, and fiber-matrix interactions were identified and solved and new materials were realized.[8] The new MMCs were expensive with marginal reproducibility; however, their use had been incorporated into 243 structural components on the space shuttle orbiters.[8] Recession in the early 1970s spurred significant research and development funding cuts which lead to the end of MMC discovery and development during this time.[8]

Development efforts were renewed on discontinuously reinforced MMCs using SiC whisker reinforcements in the late 1970s.[8] The idea of particulate reinforcement was conceptualized due to processing issues and the high expense of whiskers.[8] Particulate reinforced MMCs provided nearly equivalent strength and stiffness, but with much lower cost and easier processing.

Major advancement was made in the 1980s in both continuously and discontinuously reinforced MMCs, "major efforts included particle-reinforced, whisker-reinforced, and tow-based MMCs of aluminum, magnesium, iron, and copper for applications in the automotive, thermal management, tribology, and aerospace

industries".[8] In general, MMCs possess low coefficients of thermal expansion (CTE), high-temperature capabilities, high-specific stiffness, and high-thermal conductivity. These MMC characteristics generated excitement and optimism in the late 1980's for critical space system applications.[9] Monofilament-reinforced titanium MMCs were subsequently developed for high-temperature aeronautical systems: critical rotating components for advanced gas turbine engines and structures for high-mach airframes.[8] Although these materials were successfully inserted into specialty applications, they did not receive sufficient advertisement which prohibited a strong global impact of MMC technology awareness.[8]

A U.S. Air Force Title III program provided a significant investment to establish an MMC technology for the aerospace industry in the 1990s.[8] The U.S. Air Force Title III program inspired the production of several commercial aerospace and landmark military applications of discontinuously reinforced aluminum.[8] Additionally, new MMCs applied to ground transportation, industrial, and thermal management/electronic packaging industries experienced growth that rivaled that of the aerospace industry.[8] The MMC market for thermal management and electronic packaging was five times larger than the aerospace market in 1999. This technology gap was expected to increase through 2005 due to accelerated growth in ground transportation and thermal management markets.[8]

2.4 Composite Matrix

The composite matrix's cohesive and adhesive characteristics serve to bind the reinforcement phase together, to transfer load to and between reinforcements, and to protect the reinforcement phase from environments and handling.[8] The matrix also

provides a solid form to the composite, which allows a production part to be machined or finished in a stable manner. This is particularly necessary in discontinuously reinforced composites; the reinforcement phase is typically very fragile and is not able to maintain mechanical integrity for handling. From a structural perspective, since the reinforcement phase is stronger and stiffer, the matrix is often referred to as the composite's "weak link".[8] Due to its continuous nature, the matrix controls the transverse properties, interlaminar strength, and elevated-temperature strength of the composite.[8] The matrix also allows the reinforcement phase to be used to its maximum potential strength by enabling loads to effectively transfer from external forces to the reinforcement.[8]

In fiber reinforced MMCs, the matrix holds fibers in the proper orientation and position allowing intended loads to be carried and distributed evenly among the reinforcement phase.[8] Importantly, the matrix inherently provides an inelastic response which dramatically reduces stress concentrations and redistributes internal stresses from broken reinforcements.[8]

2.5 Composite Reinforcement

Low cost and readily available abrasive-grade ceramic grit is typical as the MMC particulate reinforcement. SiC, alumina, and boron carbide particles are used most often.[8] Titanium carbide (TiC) is commonly used for iron and titanium alloy matrices while SiC offers the best strength and stiffness for aluminum matrices.[8] "Green" SiC provides better strength and thermal conductivity than "black" SiC.[8] Alumina is slightly denser than SiC, has a higher CTE, and is more chemically stable than SiC in molten aluminum.[8]

The usage of various reinforcements has been aimed at improving mechanical properties. Nanotubes, ceramic particles, whiskers and fibers have been used as reinforcement agents throughout the history of composite development.[10-12] Many different types of fibers have been used over the course of composite manufacturing history: oxide and non-oxide type fibers such as alumina[13] and silicon carbide, respectively, tungsten or carbon substrate fibers coated with boron or silicon carbide via chemical vapor deposition, and pitch based precursors such as ployacrylonitrile (PAN) used for deriving carbon fibers.[14] Complex fibers, such as Nicalon which consist of β-SiC crystals mixed with free carbon having a composition of SiC_xO_y, with x + y being equal to four, were also used in attempts to create better composites.[14]

2.6 MMC Processing

MMCs have been fabricated using various processing techniques such as molten metal (rheo, compo, stir, or squeeze casting and various MI procedures), as well as powder metallurgy.[15,16] Carbon fiber was found to have degraded fiber-strength and poor wettability in molten Al alloys and their use was therefore limited to reinforcing OMC.[9] Due to this fact, MMC processing was directed towards sintering and diffusion based bonding[9]; giving rise to more popular processes such as melt infiltration (MI) and vacuum hot pressing.

MI techniques have become very popular due to their simplicity, cost-effectiveness, near-net shaping, homogeneous distribution of particulate reinforcement within the matrix, and easy engineering of the volumetric fraction of ceramic reinforcement products between 35 and 70 volume percent.[15] Today, the most

sophisticated material systems utilizing complex processing methods produce CMCs for high-temperature ultra-performance applications such as GE Aviation's new jet engine turbine blades. Recently, GE aviation invested $100 million dollars for a jet engine assembly facility in Lafayette, Indiana[17] based on this new generation of CMCs; composites are big business.

2.7 Previous Work: MMC

The properties of composites are critically dependent on the strengths between the matrices and reinforcing interfaces. Strong interfacial bonds are desirable as weak interfaces may fail prior to any load transferring across the matrix and reinforcement boundary. Weak interfaces may even reduce the overall matrix strength.[18]

In a recent study, two binary carbides were used to reinforce Mg-matrix composites: SiC and TiC. Magnesium has a strong affinity to wet SiC and therefore a strong, or even partially bonded, interface forms. Magnesium silicide (Mg_2Si) has been detected by X-ray diffraction (XRD) and has been previously reported as the result of a reaction between Mg and SiC.[19,20] In general, the Mg_2Si reaction particles are small and are not detected by SEM.[19-22] In contrary to the Mg-SiC reaction, Mg and TiC do not react; no Mg-Ti intermetallics exist.[23,24]

Additionally, it is known that MgC_2 forms between 400 ºC and 600 ºC [25] and becomes unstable at 680 ºC.[26] At temperatures of 500 ºC to 700 ºC, the bicarbide converts to sesquicarbide (Mg_2C_3) and at 600 ºC Mg_2C_3 decomposes into elemental Mg and carbon; the decomposition process becomes almost instantaneous at 800 ºC.[25] This

suggests that the presence MgC_2 and/or Mg_2C_3 must be limited in SiC/Mg or TiC/Mg composites because the MI temperatures are typically 750 ºC to 850 ºC.

Wetting phenomena of Mg and Al on TiC substrates was explored using the sessile drop technique.[24] A contact angle of ~120º was reported for pure Mg on TiC substrates at 850 ºC. The contact angle was reduced to a minimum of 90º when the temperature was held at 850 ºC for 30 minutes. Holding this temperature for longer durations did not decrease the contact angle.[24] The same experiment was repeated using pure Al on TiC substrates.

The initial results of Al on TiC were similar to those of Mg on TiC. However, after 90 minutes at 850 ºC, the contact angle was reduced to ~ 50º, suggesting that Al-containing Mg alloys may lead to improved wettability and more robust interfaces in TiC/Mg composites. It is worth noting that improved interface wettability stemming from Al-containing Mg alloys may not solely be the result of a chemical reaction with TiC. [26] For example, it has been shown that TiC/AZ91 composites can be synthesized via *in situ* reactive infiltration of AZ91 into an elemental mix of Ti and C, forming TiC as the only reaction product. [27-29]

MI has been used previously to synthesize Mg matrix composites with high volume fractions of reinforcements. TiC/Mg composites of 56 vol.% were fabricated via MI of pure Mg into porous TiC preforms.[23] TiC/Mg composite samples were synthesized under flowing Ar and temperatures of 850 ºC, 900 ºC and 950 ºC. Increasing the infiltration temperature resulted in increases in elastic moduli, ultimate tensile strength (UTS), and Vickers hardness from 123 to 136 GPa, 172 to 233 MPa and 183-191 to 205-

212, respectively.[23] The improvement in mechanical properties with increasing temperatures was related to Mg's better wettability at higher temperatures. It was also noted that matrix voiding and interfacial de-cohesion followed by growth and coalescence of micro-voids, generated during maximum loading, were found to be the major failure mechanism of the composites.[23]

In a similar study, 42.1 vol.% TiC/AZ91 composites were fabricated via *in situ* reactive infiltration at 800 ºC of AZ91 into TiC preforms, which were synthesized from elementally mixed Ti and C powders. These composites were reported to have a UTS of ~ 204 MPa, which was an increase of 16.2% from the AZ91 alloy without reinforcement.[27] At elevated temperatures (723 K) the UTS of the TiC/AZ91 composite was ~ 95 MPa; 180 % stronger than AZ91 alone. The failure mechanism for these composites originated from interface de-bonding[27], which mirrors Contreras et al.'s study of MI of pure Mg into porous TiC preforms.

2.8 The MAX Phases

Ti_2AlC and Ti_3SiC_2 are part of the large family of ternary carbides known as the MAX phases (Fig. 7). Many types of MAX phases were discovered in the mid-1960's through the 1990's where they were mostly ignored. In the past 15 years, however, MAX phases have been getting widespread attention.[30] More than 70 of these carbides and nitrides now exist, with more being discovered regularly. The newest additions to the MAX phase family are 413 structures (described later), solid solutions[30] and, very recently, magnetic MAX phases[31,32] which may have potential for applications in spintronics.

		A-group element				
		s^2 (group 12)	$s^2 p^1$ (group 13)	$s^2 p^2$ (group 14)	$s^2 p^3$ (group 15)	$s^2 p^4$ (group 16)
M element	**211 Phases**					
	3*d*	Ti_2CdC	Sc_2InC Ti_2AlC Ti_2GaC Ti_2InC Ti_2TlC V_2AlC V_2GaC Cr_2GaC Ti_2AlN Ti_2GaN Ti_2InN V_2GaN Cr_2GaN	Ti_2GeC Ti_2SnC Ti_2PbC V_2GeC Cr_2AlC Cr_2GeC	V_2PC V_2AsC	Ti_2SC
	4*d*		Zr_2InC Zr_2TlC Nb_2AlC Nb_2GaC Nb_2InC Mo_2GaC Zr_2InN Zr_2TlN	Zr_2SnC Zr_2PbC Nb_2SnC	Nb_2PC Nb_2AsC	Zr_2SC Nb_2SC
	5*d*		Hf_2InC Hf_2TlC Ta_2AlC Ta_2GaC	Hf_2SnC Hf_2PbC Hf_2SnN		Hf_2SC
	312 Phases					
	3*d*		Ti_3AlC_2 V_3AlC_2	Ti_3SiC_2 Ti_3GeC_2 Ti_3SnC_2		
	5*d*		Ta_3AlC_2			
	413 Phases					
	3*d*		Ti_4AlN_3 V_4AlC_3 Ti_4GaC_3	Ti_4SiC_3 Ti_4GeC_3		
	4*d*		Nb_4AlC_3			
	5*d*		Ta_4AlC_3			

Figure 7: Majority of the currently known MAX phases.[33]

The M, A, and X groups which react to form MAX phases represent three groups on the periodic table of elements (Fig. 8). The MAX phases are layered, hexagonal, early-transition metal carbides and nitrides with a general formula, $M_{n+1}AX_n$,where n = 1, 2, 3, etc.; M is an early transition metal, A is an A-group element (mostly groups 13 and 14) and X represents either carbon and/or nitrogen.[30]

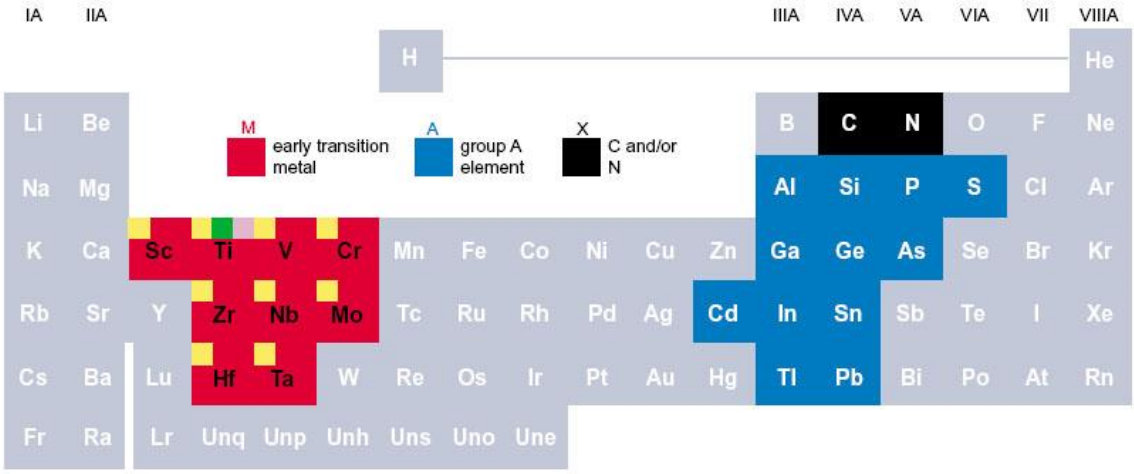

Figure 8: Elements of the periodic table that react to from MAX phases.[30]

In each MAX phase, near-close packed M layers are interleaved with layers of the pure group-A element, and the X atoms fill octahedral sites between M atoms. These octahedrally coordinated M_6X clusters are edge sharing and are identical to those found in the rock salt structure.[30] At the center of trigonal prisms, that are larger than the M_6X octahedra, the A-group elements have more space and are accommodated there.

The most apparent difference in the MAX phase crystallographic structure is the number of M layers which separate the A layers (Fig. 9). The value of *n* generates three

most common MAX crystal structures: M_2AX, M_3AX_2, M_4AX_3 where there are two, three and four M layers separating the A layers. These structures are also known as 211, 312 and 413, respectively, with the majority of MAX phases being of the 211 structure.[30]

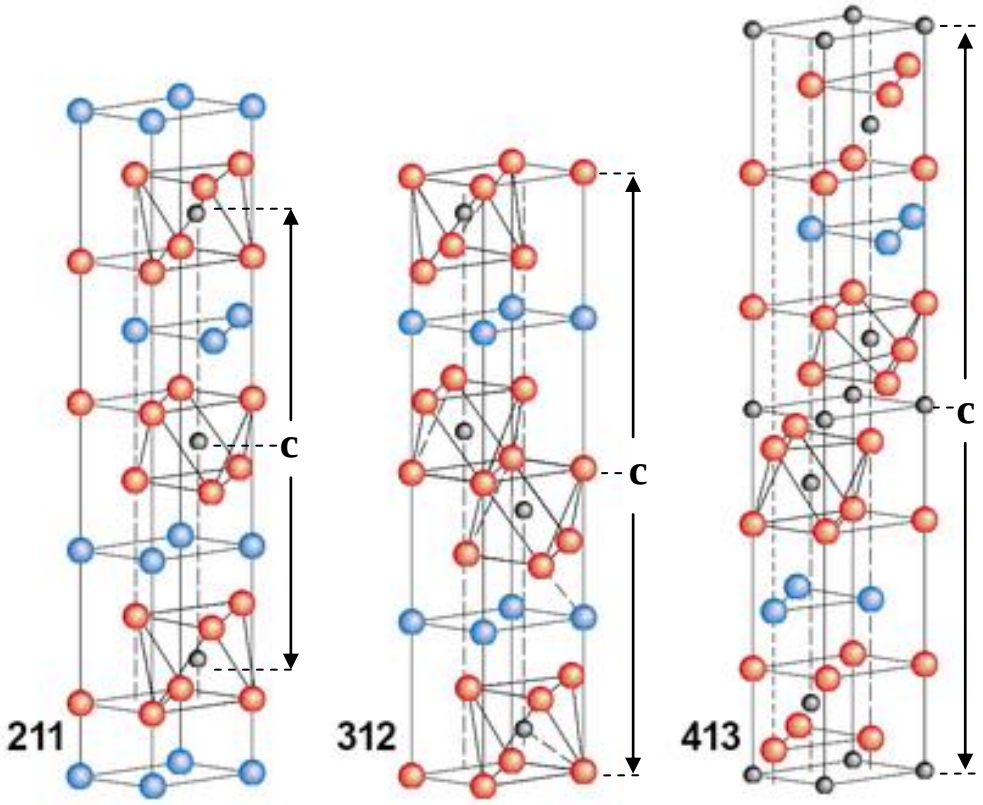

Figure 9: The unit cells of the 211, 312 and 413 crystal structures each showing its respective c-lattice parameter.[34]

The MAX phases set themselves apart as unique materials by bridging a combination of properties that are typical of ceramics and metals. Like metals, most MAX phases are readily machinable, electrically and thermally conductive, plastic at high temperatures, highly damage tolerant and resistant to thermal shock.[26,30] For

example, Ti_3SiC_2 was so resistant to thermal shock that quenching in water from 1400 ºC caused a slight increase to its flexural strength when in comparison to unquenched samples.[30] Some MAX phases compare with ceramics in that they are elastically rigid (Young's Moduli > 300 GPa), lightweight (~4 to ~5 Mg/m^3), are oxidation resistant and maintain their mechanical strengths to higher temperatures. Ti_2AlC is also creep, fatigue and oxidation resistant.[26] Cr_2AlC has become a material of interest due to its excellent oxidation resistance and high CTE; NASA has ongoing work with hopes that it has potential for applications in thermal barrier protective coatings.

The MAX phases are highly plastically anisotropic due to their large c/a lattice parameter ratio. The plastic anisotropy is a direct result of dislocations being confined to the basal planes at all temperatures.[26] MAX phases are considered kinking non-linear elastic (KNE) solids which are characterized by nested, fully reversible hysteresis stress-strain loops (Fig. 10).

When KNE solids are subjected to cyclic loading, dislocation loops nucleate and grow on slip planes and during unloading they shrink and annihilate.[30,35,36] These materials are called "kinking" because they have a tendency to kink as they deform. They are termed "non-linear" because they show non-linear stress-strain behavior during loading and unloading. KNE solids are also termed "elastic" because there is no permanent deformation observed during cyclic loading. Therefore, this reversible dislocation motion causes energy dissipation during cyclic loading and the area within a closed hysteresis loop is a measure of the dissipated energy these materials are capable of. For instance, Ti_3SiC_2 has shown to dissipate 25% of the mechanical energy during

high stress (1 GPa) cyclical loading.[35] As a result of this behavior, MAX phases are of special interest for cyclic compressive applications.

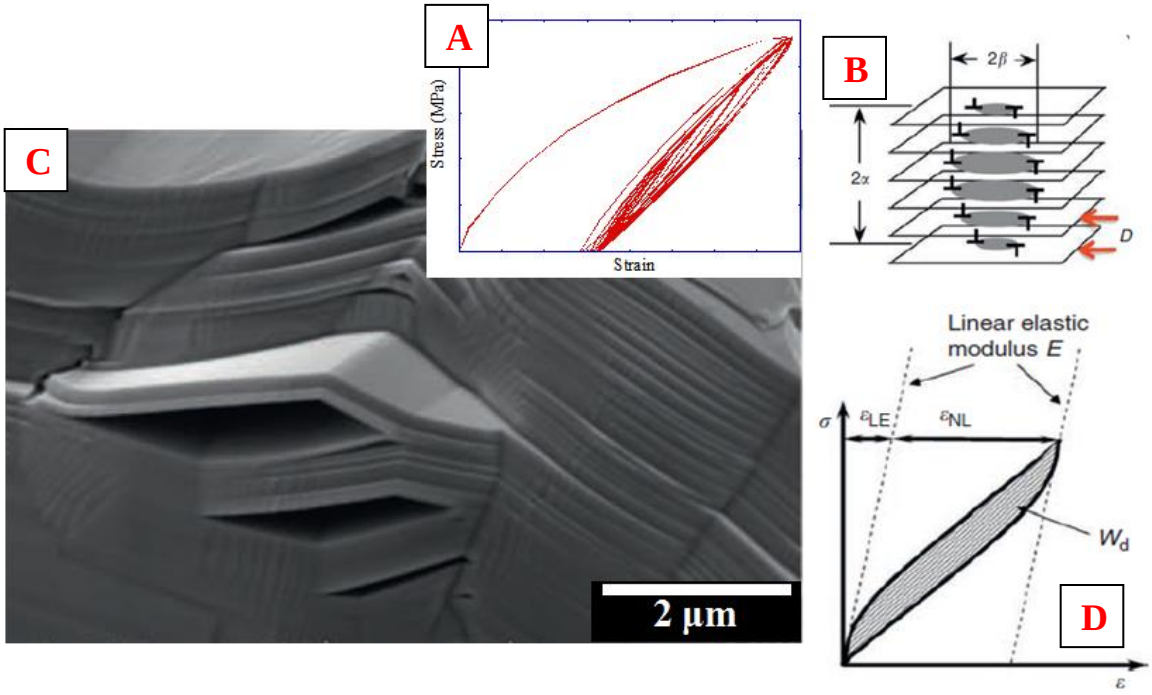

Figure 10: Nested hysteresis loops in a stress strain curve showing tell-tale signs of energy dissipation (A); dislocation loops which open and close during loading and unloading (B); kinking material under stress (C); non-linear stress-strain behavior which exhibits elasticity and no deformation (D).

2.9 Previous Work on MAX/Mg-Alloy Composites

More recent studies have taken advantage of MAX phases as the reinforcement phase in MMCs. Pressureless MI of Mg into ~ 50 vol.% porous Ti_2AlC preforms, leading to the synthesis of Ti_2AlC/Mg composites with excellent mechanical properties and good dampening capability, was first fabricated by Amini *et al.* [37] The Ti_2AlC (50 vol.%)/Mg

composites have ultimate compression strength (UCS) and UTS of 700±10 and 345±40 MPa, respectively. The reported mechanical properties for the Ti_2AlC (50 vol.%)/Mg composites were higher than those reported for Ti_3SiC_2 (50 vol.%)/Mg and SiC (50 vol.%)/Mg composites. The Ti_2AlC composites system also exhibited ultra-high damping while being light ($2.9g/cm^3$).[38] The Ti_2AlC (50 vol.%)/Mg composite's high mechanical properties were attributed to the presence of nanocrystalline Mg grains within the composite matrix as characterized by TEM.[38]

More current work by Anasori *et al* has shown Ti_2AlC/Mg-alloy and TiC/Mg-alloy composites to result with excellent mechanical properties. This work studied the effect of the Al wt. % content in the composites matrix and the effect of coarse and fine MAX phase reinforcement particle grain size. Maximum yield strengths (YSs) of 426±5 and 768±11 MPa were reported for the fine grained (FG) FG-Ti_2AlC/AZ61 and FG-TiC/AZ91 composites, respectively. Maximum UCSs of 773±7 and 1028±5 MPa were reported for the FG-Ti_2AlC/AZ31 and FG-TiC/AZ61 composites, respectively.[26]

The mechanical properties in the 2013 work by Anasori *et al* were shown to increase significantly with increasing amounts of Al wt. % content in the matrix (Fig. 11). The UCS's rose from 688 ± 18 to 768 ± 11 MPa in the FG-Ti_2AlC/AZ alloy composites when the Al content increased from 0 to 9 wt. %.[26] In the same composite, YSs rose from 349±3 to 408±4 MPa when Al increased from 0 to 9 wt. %.[26] With Al wt. % changing from 0 to 9% in the FG-TiC/AZ alloys, its respective UCSs and YSs rose from 705 ± 10 to 1013 ± 12 MPa and 421 ± 10 to 557 ± 8 MPa.[26] Clearly, a strong

correlation between increasing mechanical properties and additions of Al wt. % in the matrix exists.

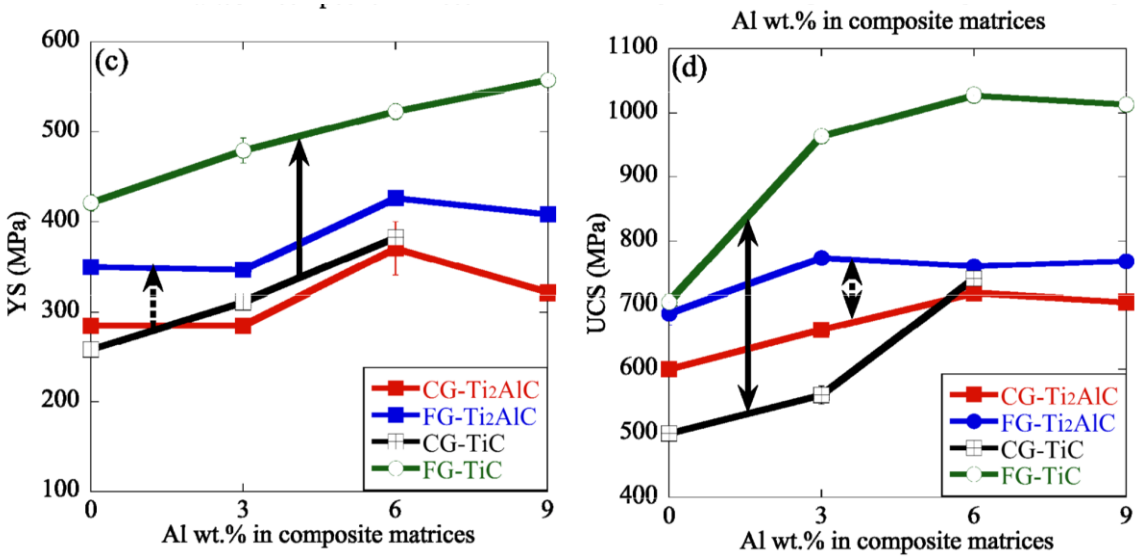

Figure 11: YS and UCS results from Anasori *et al's* work on fine and coarse reinforcement particle grain size MMCs.[26]

2.10 Objective of this Work

Coupling the evidence that Mg shows promise by being light weight with exceptional damping capability, and that Al has been reported to promote stronger interfaces in these composites, the AZ series Al-containing Mg-alloys were selected as the matrix materials. Furthermore, previous work has shown Al-containing Mg-alloys to have better mechanical properties in composites than pure Mg as the matrix. Additionally, the AZ series alloys were chosen because they are commercially available and popular in scientific literature.

MAX phases were chosen for two reasons: 1) previous work has shown increased mechanical strengths with their use; 2) ease of machinability in comparison to SiC or TiC. Therefore, it was desirable to consider alternative MAX phase reinforcements which appeared attractive for this work. To most effectively probe the intriguing mechanical phenomena at hand, careful consideration of MAX phases with different M-element and A-group element MAX constituents other than Ti and Al, respectively, were selected to be explored.

In Amini *et al's* study, the UCS for Ti_2AlC/Mg composites were reported at 700 ± 10 MPa; higher in comparison to the UCS from the SiC/Mg and Ti_3SiC_2/Mg composites reported at 500 ± 25 MPa and 460 ± 10 MPa, respectively.[37] Although the preliminary work on the Ti_3SiC_2/Mg composite has shown lower mechanical properties, the Ti_3SiC_2 reinforcement showed promise strong enough for its consideration in this work. Using Ti_3SiC_2 instead of Ti_2AlC effectively changes the A-group element to Si from Al. Additionally, Ti_3SiC_2 powder was chosen because it is commercially available and quite stiff.[39]

It was an attractive idea to replace Ti with Cr as the M-element. Therefore, Cr_2AlC was chosen. Cr_2AlC has a relatively high CTE ($1.3X10^{-5}$ K^{-1})[40] when compared to most other MAX phase cousins. Cr_2AlC's CTE is much closer to that of Mg's ($2.6X10^{-5}$ K^{-1}) and it is thought that by using a MAX phase with a CTE, closer to the CTE of Mg, there will be less interface mismatch resulting in less interfacial residual strain. It is hypothesized that Cr_2AlC/Mg-alloy composites may experience less issues during elevated temperature environments. Because of these reasons, coupled with the

argument that no existing work regarding Cr_2AlC/Mg-alloy composites is known of, Cr_2AlC was an appropriate choice.

Considering the choice of these materials and the direction paved by the previous work, the objective for this work was been clearly defined: exploit melt infiltration of Mg-alloys into porous MAX phase carbide preforms as an approach to develop advanced materials which show promise to satisfy the stringent demands of the military and various industrial sectors. This research on MAX phase/Mg-alloy composites is promising because of their higher strengths and stiffness values, lighter weights and ease of machinability. The primary goal of this work was to explore two new composite systems that have never have been fabricated before. The hope of this work was to lessen the amount of time necessary to identify and create new materials which satisfy the ever increasing demands on a broad sector of industries. Additionally, it was hoped that this work would shed light upon a deeper understanding between the connection of mechanical properties and the MAX phase reinforcement particle's interaction with the Mg-alloy matrix.

3. Materials

3.1 Composite Matrix: Mg and Mg-alloys

This work is based on the following composites, all of which were at a matrix loading of ~45 vol. %: Ti_3SiC_2/Mg, Ti_3SiC_2/AZ31, Ti_3SiC_2/AZ61, Ti_3SiC_2/AZ91, Cr_2AlC/Mg, Cr_2AlC/AZ31, Cr_2AlC/AZ61, Cr_2AlC/AZ91. Pure Mg (99.8% pure), AZ31B (3 wt.% Al, 1 wt.% Zn) both purchased from Alfa Aesar (Ward Hill, MA) and AZ61L (6 wt.% Al, 1 wt.% Zn, low Mn) and AZ91D (9 wt.% Al, 1 wt.% Zn) both supplied by Thixomat (Livonia, MI) were used.

3.2 Composite Reinforcement: MAX phases

Powder Ti_3SiC_2 was purchased (Kanthal, Sweden). The Cr_2AlC powders were synthesized in-house. The Cr_2AlC powder was synthesized starting with Cr powder (Alfa Aesar, -325 mesh, 99% pure, stock # 10148) Al powder (Alfa Aesar, -325 mesh, 99.5% pure, Stock # 11067), and graphite powder (Alfa Aesar, -300 mesh, 99.0% pure, stock # 10129).

4. Processing & Experimental Methods

4.1 Preparation of Carbide Powders

Approximately 500 g of the as-received -325 mesh Ti_3SiC_2 powder was placed into a 500 mL plastic bottle (US Plastic, Lima, OH.) along with ~25 10 mm zirconia milling balls (Inframat® Advanced Materials, Manchester, CT.). The 500 mL bottle was capped and placed into a ball milling container and was subsequently milled for ~ 24 h at 60 rpm. The mixed powders were subsequently sieved and ball milling/sieving was repeated until ~ 400 g of - 400 mesh powder was created to synthesize all four Ti_3SiC_2 reinforced MMC's.

The Cr_2AlC powder was synthesized by mixing elemental powders in the molar ratio 2:1.1:1. The weight percentages used were: Cr (71.38%), Al (20.37%), C (8.24%). Approximately 500 g of elemental powder was ball milled for ~24 h at 60 rpm using ~ 25 10 mm zirconia milling balls. The ball milled elemental powder was placed into a flat bottomed cylindrical alumina crucible (AdValue Technology, Tucson, AZ) with inner (I.D.) and outer diameters (O.D.) and height of 66, 74 and 150 mm, respectively. The crucible was capped with a circular alumina lid of diameter ~ 80 mm and was placed into a graphite heated, vacuum-atmosphere hot press (HP) (Series 3600, Centorr Vacuum Industries, Somerville, MA). Subsequently, the crucible was heated at a rate of 300 °C/h until 1400 °C where it was held at that temperature for 1 h. The furnace was cooled at 500 °C/h to ambient temperatures.

In making powders, it is important to keep the heating rate low. Too fast of a heating rate can cause a self-propagating high temperature reaction – i.e. the powders ignite. In extreme cases, this run away reaction can cause damage to laboratory equipment. The heating rates also depended on the amount of material being reacted. For 450 g, 600 g and 700 g batches of elemental powders the heating rates were, 300 °C/h, 125 °C/h and 100 °C/h, respectively. The flat bottomed cylindrical alumina crucible with inner and outer diameters and height of 66, 74 and 150 mm, respectively, was used. Powder bed heights corresponding to the 450 g, 600 g and 700 g batches of elemental powders were ~ 67, 90, and 105 mm, respectively. These heating rates resulted in the production of high purity Cr_2AlC bricks. The bricks were milled into a fine powder using a semi-automated milling machine (Bridgeport Machines Inc., Brigdeport, CT.) equipped with a 7.62 cm diameter shell-inserted tungsten carbide mill that swept across the MAX brick surface in height decrements of 0.64 mm per sweep (Fig. 12). The milled fine powder was then subject to the same ball milling and sieving procedure as discussed above. This process was repeated until ~ 400 g of -400 mesh powder was obtained; ensuring enough to synthesize all four Cr_2AlC reinforced MMC's.

Figure 12: 7.62 cm diameter shell-inserted tungsten carbide mill

4.2 Preparation of Carbide Preforms

Porous Ti_3SiC_2 (54 ±1 vol. % dense) and Cr_2AlC (55 ±1 vol. % dense) preforms were synthesized using the same process. A cylindrical graphite die of height ~170 mm, width of ~ 114 mm and centerline vertical bored diameter of ~40 mm was used to house the preform (Fig. 13). The die's bore was lined with a rolled section of graphite foil. Three graphite punches were coated with boron nitride spray; two of them having a height of 70 mm, the other having a height of 40 mm, and all with diameters of 38 mm.

The lowermost 70 mm high coated punch was slid into the graphite foil-lined die bore until it sat flush with the bottom of the die. Four 38 mm graphite foil discs were cut

out of a graphite foil sheet and were subsequently pushed down the bore to lie on top of the lowermost punch. Approximately 60 grams of the sieved - 400 mesh MAX phase composite reinforcement powder was poured into the graphite die bore in 10 gram batches. After every 10 gram addition, the die was gently tapped on the workstation table a few times to ensure the elimination of voids or gaps in the powders. The die was, however, not tapped too much as to orient the MAX powders, as a random orientation of particles was desired to give rise to composites with uniform mechanical properties in all directions. After the last 10 gram addition, four more 38 mm graphite foil discs were pushed down the die bore to lie atop the powder. The 40 mm high boron nitride coated graphite punch was subsequently slid down the graphite die bore. The second 70 mm high boron nitride coated graphite punch was then inserted to complete the set-up for creating the MAX preform.

Figure 13: Picture of graphite die with a 70mm high boron nitride coated punch extending out of the die bore.

Once the die was prepped, it was placed in the HP. To synthesize Ti_3SiC_2 preforms, the HP was heated to 1100 °C, at a rate of 500 °C/h, and held at 1100 °C for one hour. The application of pressure was programmed to ramp-up with loads corresponding to a rate of ≈ 70 MPa per hour starting at approximately 900 °C, reaching a maximum pressure of 13.8 MPa and holding this pressure throughout the peak temperature holding time. The addition of pressure results in green-bodies with enhanced strengths that are needed to prevent fracture during MI. This program produced porous Ti_3SiC_2 (54±1 vol. % dense) preforms with heights and diameters of ≈ 18 mm and 38 mm, respectively. The density of a sintered preform was found by measuring the mass on a calibrated scale and the height and diameter with a caliper to calculate the volume. Four preforms were made and measured to get find the average and standard deviation.

To synthesize Cr_2AlC preforms, the HP was heated to 900 °C at a rate of 500 °C/h and held at 900 °C for one hour. This procedure produced porous Cr_2AlC (55±1 vol. % dense) preforms with heights and diameters of ≈ 18 mm and 38 mm, respectively. Because no pressure was used to synthesize the Cr_2AlC preforms, the sintered green bodies were more fragile and careful handling was required during subsequent processing steps.

Both HP programs were operated under ~10 Pa vacuum, and had a cooling rate of 500 °C/h. After the samples were relatively cool, the HP was turned off. A controlled and slow cooling rate from peak temperature for the first few hours is important to let the material relax; not shocking the sintered green-body preforms.

It should be mentioned that the composites synthesized herein will henceforth be labeled according to the following convention: MAX phase reinforcement type/(MAX phase reinforcement volume % density)/Matrix. For example, the 55 vol. % Cr_2AlC/Mg composite will be referred to as Cr/55/Mg; the 54 vol. % Ti_3SiC_2/AZ91 composite will be referred to as Ti/54/91, etc.

One of the findings of this work is that the green body relative density is an important factor which can have quite an effect on the mechanical properties in these materials, as will be discussed and shown later.

4.3 Pressureless Melt Infiltration

MI was performed in the same vacuum HP that the carbide preforms were synthesized in. The MI process was the same for all composite samples. The process began by using a flat-bottomed cylindrical alumina crucible (AdValue Technology, Tucson, AZ) of dimensions: O.D. (60 mm), I.D. (54 mm) and 100 mm high.

The crucible interior surfaces were lined with graphite foil to prevent any reaction between the Mg-alloys and alumina; the carbide preform was carefully placed inside the crucible. Mg or Mg-alloy flakes, chunks or small slices were then placed on top of the preform. Cut-outs of graphite foil discs and graphite foil tabs were placed over the metal chunks to aid in preventing the Mg or Mg-alloy vapor from escaping the local melt infiltration environment inside the crucible (Fig. 14). A 10 cm^2 piece of graphite foil was used to separate the alumina crucible lid from the alumina crucible. The entire assembly was then placed inside the graphite-heated vacuum furnace. A graphite die weighing ~ 1

kg was put on top of the crucible lid and the HP hydraulic ram was lowered to put pressure on the lid. This was done to ensure a reduced loss of Mg or Mg-alloy vapor. The vacuum furnace door was closed and locked; vacuum was pulled until ~ 10 Pa pressure was reached.

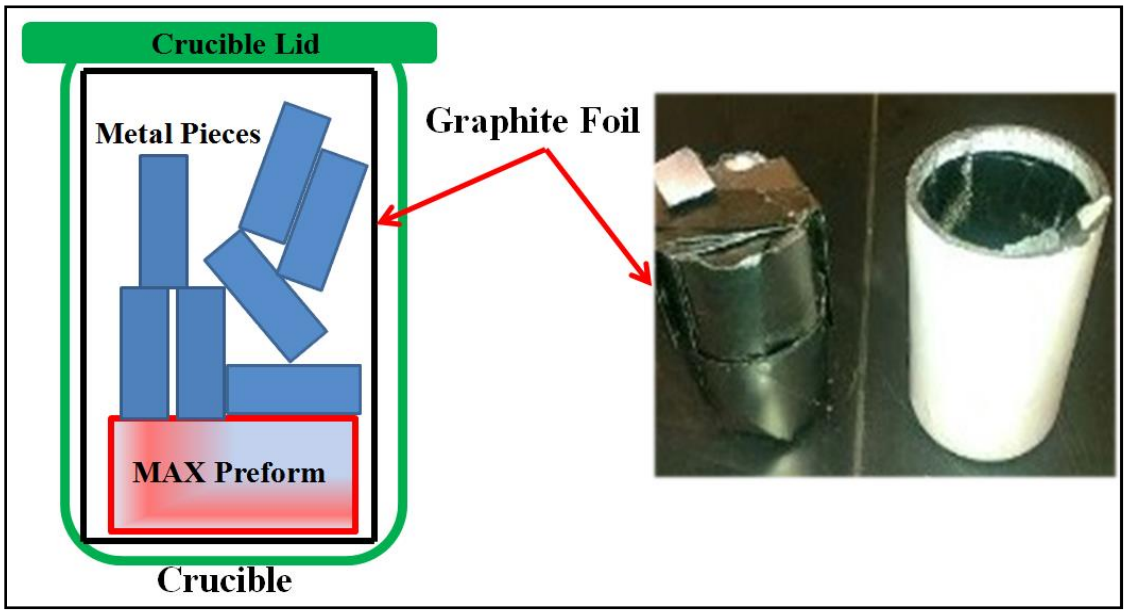

Figure 14: MI prep schematic and actual set-up.

The HP was heated at a rate of 500 °C/h to 750 °C and held at that temperature for 1.5 h before the cooling sequence began at 500 °C/hl. The high vapor pressure of Mg, or Mg-alloys, resulted in metal condensing on the graphite foil between the alumina crucible lid and walls creating a good seal. Previously, the same procedure was performed with no graphite foil sheet separating the crucible and its lid.[26] This practice frequently led to having to break the crucible open to extract the composite sample. The

purpose of the graphite foil separator allows the crucible lid to be taken off easily and prevents having to break the crucible in order to remove the finished MMC.

4.4 MMC Sample Preparation and Archimedes' Principle

Once the sample was removed from the crucible, any extraneous metal was ground off (Struers Rotopol-22, Struers Rotoforce-4, Cleveland, OH) using 80 grit sandpaper (Allied High Tech, Compton, CA.) and water. The sample was then vacuum heat dried for one hour at ~ 140 °C. Archimedes' principle was subsequently performed to confirm that the samples were 95 % dense or better.

To calculate the relative densities, the following densities were used: 4.52 gcm^{-3} and 5.24 gcm^{-3}, for Ti_3SiC_2 and Cr_2AlC respectively.[33] Magnesium has a density of 1.74 gcm^{-3} while AZ31, AZ61 and AZ91 have densities ranging from ~1.71 to ~1.81 gcm^{-3}, respectively.[41] Three equations were used to find composite relative densities:

$$\rho_{A.P.} = M_{dry} / (M_{sat} - M_{wet}), \qquad 1$$

where $\rho_{A.P.}$ is the Archimedes density, and M_{dry}, M_{sat} and M_{wet} are the dry, saturated and wet masses of the composite;

$$\rho_{Theor.} = Vf_{MAX}(\rho_{MAX}) + Vf_{matrix}(\rho_{Matrix}), \qquad 2$$

where $\rho_{Theor.}$, ρ_{MAX} and ρ_{Matrix} are the composite's theoretical, MAX phase, and matrix densities, respectively. Vf_{MAX} and Vf_{matrix} are the respective MAX phase reinforcement and matrix volume fractions in the composite. Lastly, the % density of the composite was found by dividing the Archimedes and theoretical densities.

$$\% \text{ Density} = \rho_{A.P.} / \rho_{Theor.} \qquad 3.$$

The relative densities of the composites fabricated in this work were tabulated (Table 1). The error in the relative density is due to carried uncertainty associated with caliper measurements on non-uniform heights and diameters used for calculating the MAX phase preform volume % density.

Table 1: Relative density (gcm^{-3}) of composites fabricated in this work measured using Archimedes' principle.

Sample	Mg	AZ31	AZ61	AZ91
Ti_3SiC_2	3.25 (99±1%)	3.29 (99±1%)	3.23 (99±1%)	3.27 (99±1%)
Cr_2AlC	3.70 (99±1%)	3.64 (99±1%)	3.72 (99±1%)	3.71 (99±1%)

4.5 Microstructural Characterization

Each MMC was cross-sectioned (Struers Accutom-5, Cleveland, OH.) using a diamond wafering blade (Allied High Tech products, #60-20080, Compton, CA.), hot mounted (Struers LuboPress-3 Cleveland, OH.) in hard black epoxy (Allied High Tech products, #150-10105, Compton, CA.), and subsequently polished down to a 1 μm surface using diamond slurry (Allied High Tech, Compton, CA.). Polished surfaces were imaged by SEM (Zeiss Supra 50VP, Germany) equipped with an energy dispersive spectroscope (Oxford Inca X-Sight, Oxfordshire, UK).

The XRD patterns were obtained using a diffractometer (Rikagu Smartlab, Japan) with step scans of 0.02° in the range of 5° to 80° 2-theta and a step time of 1 s, with a 10

mm^2 window slit. Cu K_α radiation (40kV and 30mA) was used. The broad 2-theta range was used in order to help identify any additional phases from reactions, such as intermetallics or carbides, created during the MI process. Jade XRD pattern recognition software (Materials Data, Inc., Livermore, CA.) was used to verify the XRD results.

4.6 Vickers Microhardness

Vickers microhardness measurements were made using a Vickers hardness indenter (LECO Corp., St. Joseph, MI) under a 9.81 N force with a 10 s dwell period. Ten indentations were made. These measurements were averaged and standard deviations were found for each composite sample.

4.7 Compression Testing

Compression specimens were electro-discharge machined (EDM) from each MMC sample. The orientation of each EDM burn can be considered as negligible since the carbide powders were synthesized in a random orientation. Six cubes of dimension 4 mm^3 for UCS testing and one cylinder with 9.7 mm diameter and 31 mm height for cyclic compression testing were EDMd from each composite sample.

The cubes were loaded until fracture by displacement (Fig. 15A) on an electromechanical testing machine (Instron 5600, Norwood, MA). Each EDM cylinder was cyclically loaded in compression in order to determine yield strengths and effective moduli. An extensometer (2620-603 Instron, 10 mm gauge length with a 10% full range) was attached directly to the cylinder to measure strain. The starting stress for cyclic testing was approximately 65% of the maximum UCS for each sample as determined by

compressing the 4 mm^3 cubes to failure. This was done to guarantee that the cyclic compression samples would not be destroyed. At 65% of the maximum UCS, each cyclic compression ran to a maximum of either 400 or 350 MPa and ran with subsequent cycles in decrements of 50 MPa down to 100 MPa (Fig. 15B).

The first loop of the cyclic compression test exhibits an open loop having a small plastic strain amounting to 0.5 to 2.0%. Typically, after the first two cycles, the subsequent decremental loops are closed (Fig. 15B). The stress-strain loops signify energy dissipation which is due to reversible dislocation motions.[26,42]

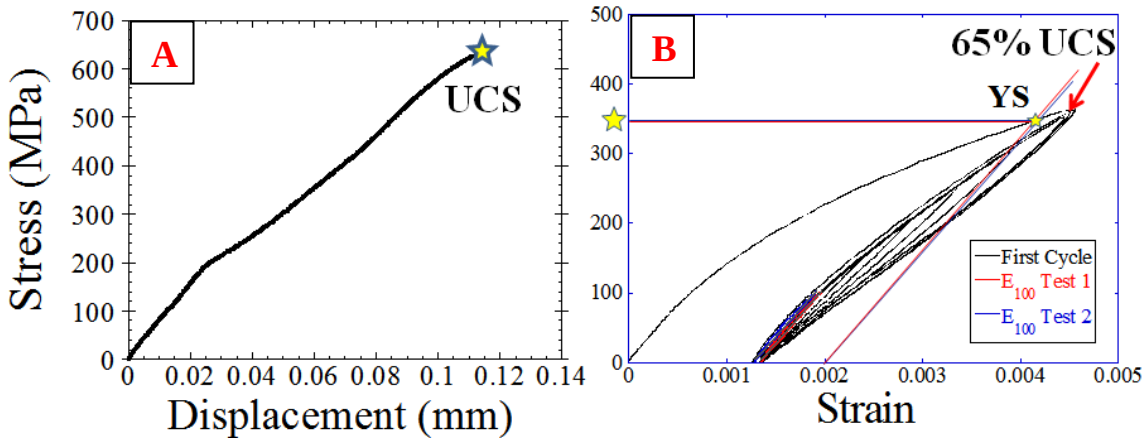

Figure 15: UCS found by displacement testing (A); example showing how YS was found and the closed hysteresis loops in cyclic compression testing (B).

4.8 Elastic Moduli and Yield Strength

It is assumed that since both types of all the composites in this work were synthesized using -400 mesh MAX powder, and the exact same Mg and Mg-alloys, the reinforcement particle size and melt infiltrated matrix materials can be considered

consistent. Therefore, the rule of mixtures or Halpin-Tsai methods, [19,26] to estimate the composite elastic modulus were not used. Estimates of the elastic moduli were found by fitting a linear regression to each closed hysteresis loop (Fig. 16). The slopes of the linear regressions are based on the simple relationship:

$$E_{eff(avg)} = \frac{\sigma}{\varepsilon} \qquad 4$$

where the effective modulus, $E_{eff(avg)}$, is equal to the stress, σ, divided strain, ε. The slopes of these loops were averaged and the standard deviations were calculated to report $E_{eff(avg)}$.

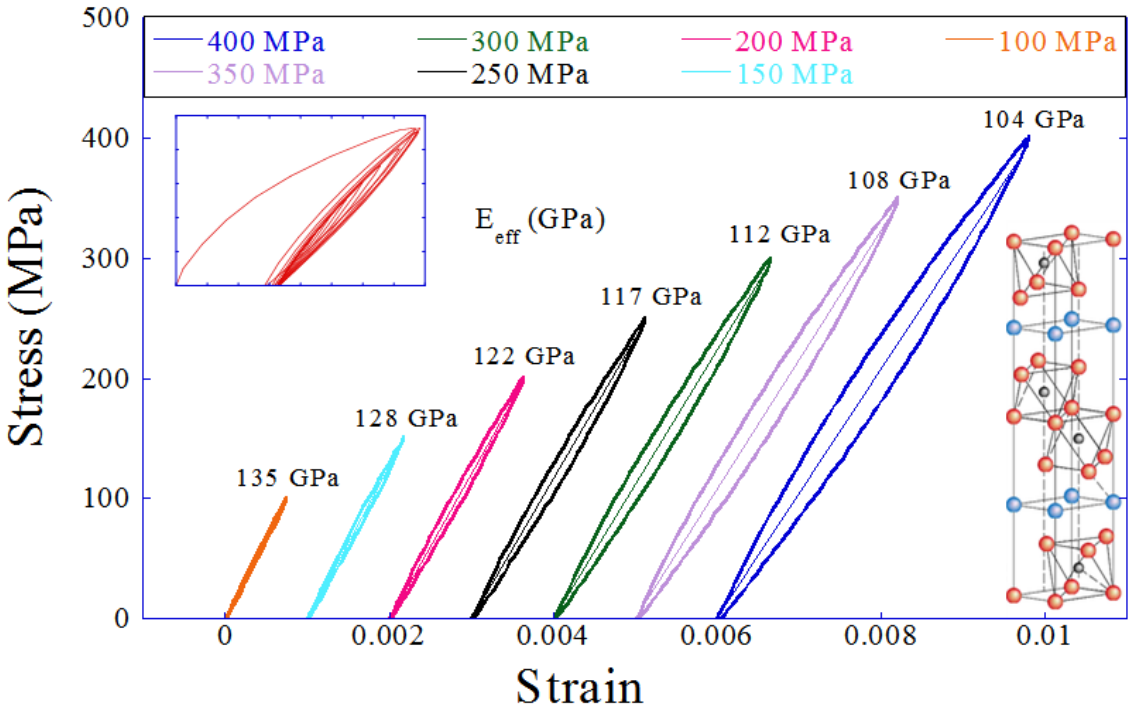

Figure 16: Fully reversible closed hysteresis loops being separated for exemplifying how composite effective moduli were found.

Fully reversible hysteresis loops are only observed at stresses of 100 MPa or higher; below these stresses, the stress-strain curves are linear.[26] Due to kinking non-linear elastic phenomena in the composite materials in this work, the linear elastic region in a stress-strain curve is not identifiable. This is because dislocations begin to move, resulting in micro-yielding, at the onset of applied stress. This eliminates any easily identifiable linear elastic region at the beginning of the stress-strain curve. This slope of the linear elastic region in common materials, such as metals, is taken as the materials elastic modulus. This slope can also be transposed to 0.2% strain from where a yield strength estimate can be found. In these micro-yielding materials, estimating YS in this way is not possible and this is ultimately why the true moduli of these composites must be estimated as effective moduli where the effective modulus is defined as the combination of elastic and plastic effects in an overall stress-strain relationship service structure.[43] Due to the sensitivity of the Instron testing equipment, the slopes of the 100 MPa hysteric loops (Fig. 15B) were used as the best estimate to the true elastic modulus and are reported as $E_{100(avg)}$.

Two cyclic tests were run at 65% of the maximum UCS on each composite sample. The slope from each 100 MPa loop was transposed onto one stress strain curve at 0.2% strain (Fig. 15B). Where the slopes intersected the stress-strain curve provided the estimate of the composite YS (Fig. 15B). Any difference between the intersections on the stress-strain curve by the two slopes from the 100 MPa loops was used as the error associated with the YS measurement.

5. Results

5.1 XRD: In-house Synthesized Cr_2AlC Powder

XRD was performed on the in-house synthesized Cr_2AlC -400 mesh powder (Fig 17). The diffraction peaks were subsequently characterized using Jade XRD software. A small addition of silicon (~ 5 wt. %) was added to the Cr_2AlC powder to be used as an internal standard. The small peak observed at ~ 28° 2-theta corresponds to the added Si powder. The powder was found to be quite pure, with all experimental peaks corresponding to the reference data. Very small $Cr_{23}C_6$ peaks corresponding to ~ 1% by volume were found to exist.

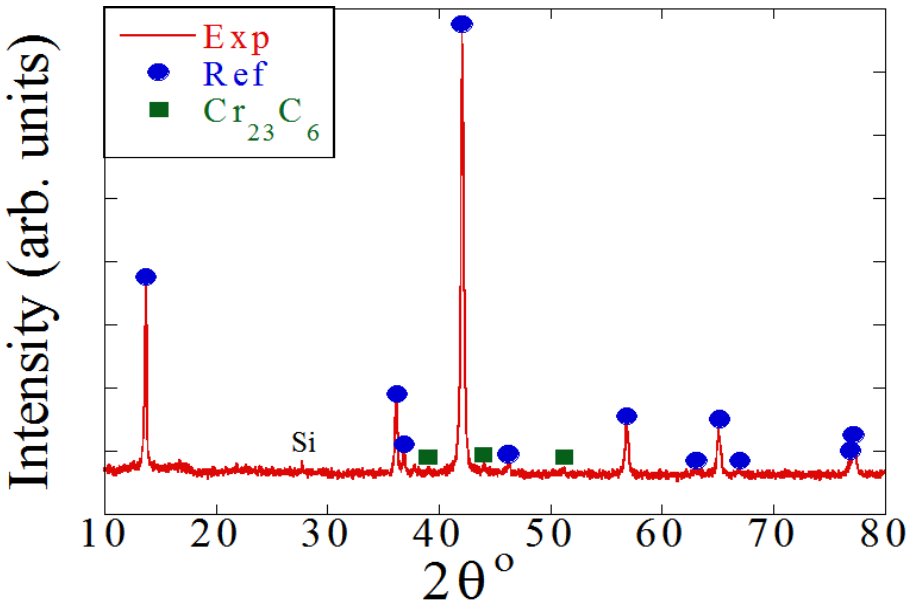

Figure 17: In-house synthesized Cr_2AlC powder XRD pattern matched to the JADE XRD database reference.

5.2 XRD: Cr_2AlC reinforced Mg Composites

A thin parallel plate was cross-sectioned from the Cr/55/Mg composite, was subsequently polished with 800 grit sandpaper and then XRD was performed. A large chunk was also cut from the Cr/55/Mg composite and was annealed at 750 ºC for 24 h under an Ar atmosphere. A thin parallel plate was then cross-sectioned from this sample and its XRD pattern was collected. By comparing the pre- and post-annealed XRD patterns, no changes were discerned (Fig. 18). No reaction phases were found as a result of annealing. The black vertical lines spanning the two spectra indicate $Cr_{23}C_6$ peaks (Fig. 18).

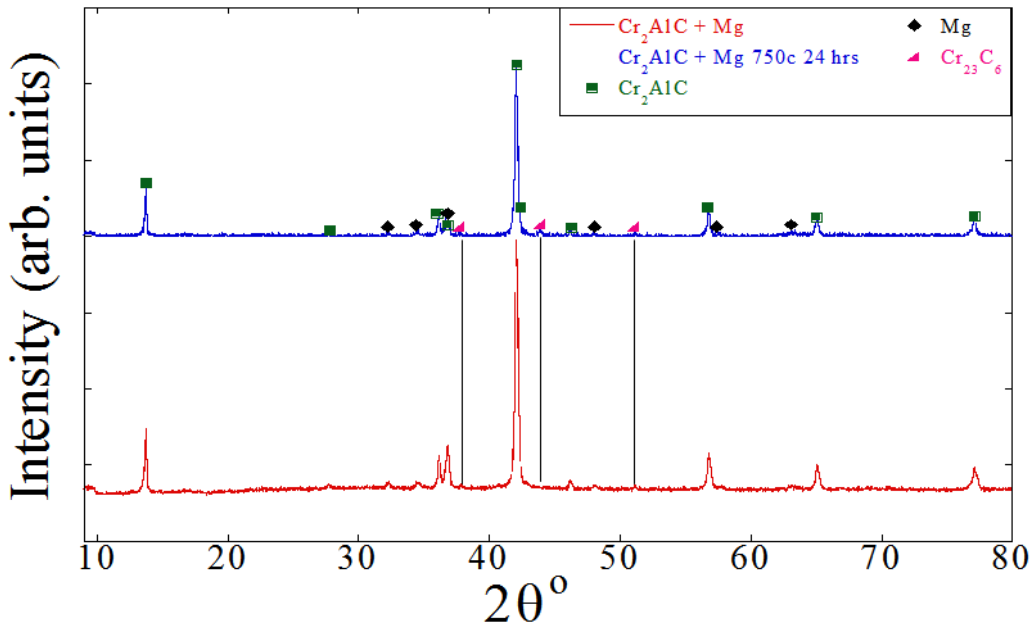

Figure 18: Overlayed XRD patterns for the Cr/55/Mg composite before (bottom curve) and after (top curve) annealing for 24 h at 750 °C.

5.3 XRD: Ti_3SiC_2 reinforced Mg Composites

A thin parallel plate was cross-sectioned from a Ti/55/Mg composite sample and was subsequently polished with 800 grit sandpaper. A large chunk was also cut from the Ti/55/Mg sample and was annealed at 750 ºC for 24 h under an Ar atmosphere. XRD patterns of both samples were obtained (Fig. 19). Each peak was accounted for when characterizing the Ti/55/Mg composite in the pre- and post-annealed conditions. Several small peaks at ~ 24º and ~ 40º 2-theta were characterized as magnesium silicide (Mg_2Si). Titanium carbide peaks were observed in the spectra and were expected to be present as a processing by-product reaction during Ti_3SiC_2 powder manufacturing. No reaction phases were found as a result of annealing.

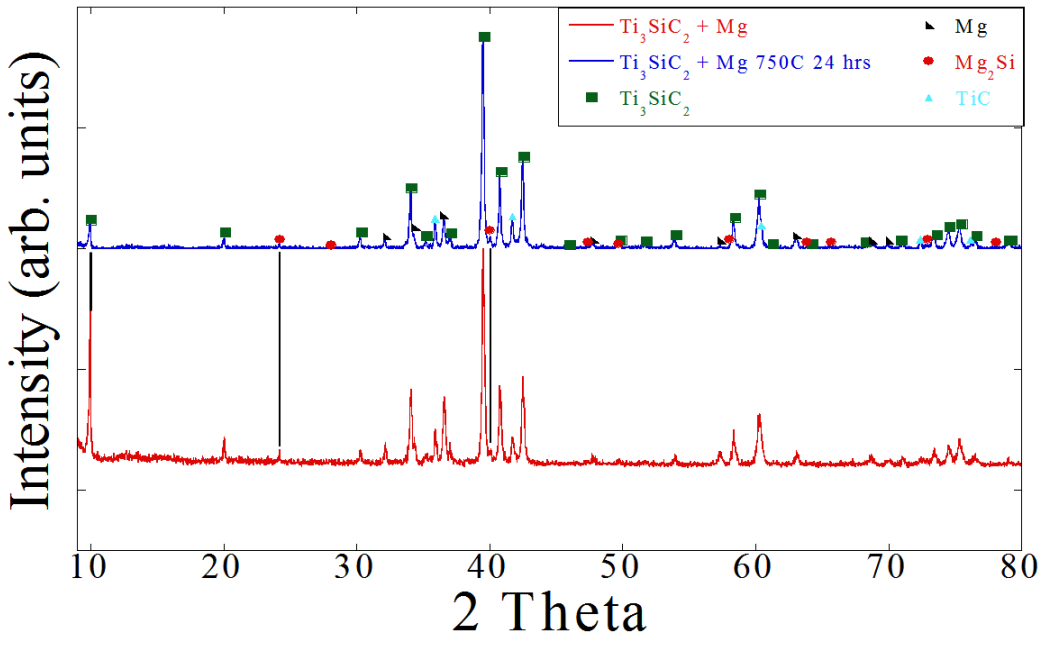

Figure 19: Overlayed XRD patterns of the Ti/55/Mg sample before (bottom curve) and after (top curve) annealing for 24 h at 750 °C.

A Ti/55/91 XRD sample was prepared as a thin parallel plate cross-section. XRD results from the Ti/55/Mg and Ti/55/91 composites were compared (Fig. 20). Several peaks observed at ~ 24°, ~ 29° and ~ 40° 2-theta were characterized as Mg_2Si. The black vertical lines spanning the two spectra in indicate the three Mg_2Si peaks at ~ 24°, ~ 29° and ~ 40° 2-theta (Fig. 20).

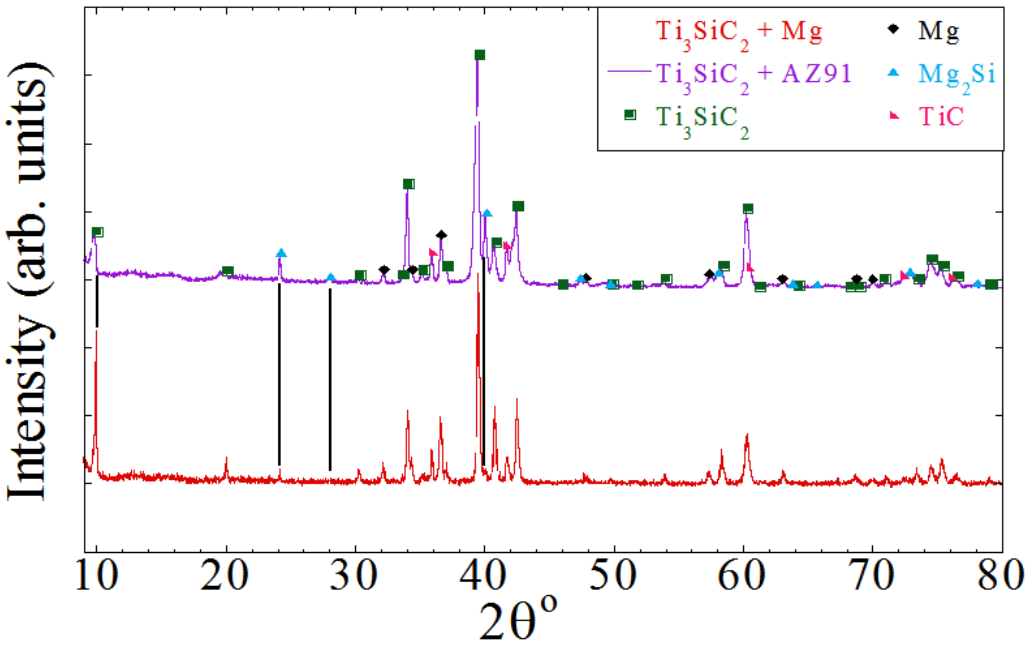

Figure 20: Overlayed XRD patterns of the Ti/55/Mg sample (bottom curve) and Ti/54/91 (top curve).

5.4 Pre-stress Evaluation of Microstructure

Each MMC sample showed a homogenous distribution of reinforcement particles in the composite matrix. The matrix material in the majority of the following images has been pulled out of the composite due to the grinding and polishing procedure. In each SEM image, the MAX phase reinforcement of the composite can be seen as the light grey

areas. In higher magnification images, the kinked and delaminated microstructure inherent to MAX phases becomes clearly visible.

Ti/55/31and Ti/55/Mg composites were imaged in secondary electron (SE) mode and have been labeled to indicate regions of MAX phase reinforcement particles and matrix areas (Fig. 21). The microstructure of the Ti_3SiC_2 reinforced composites show an elongated rectangular morphology.

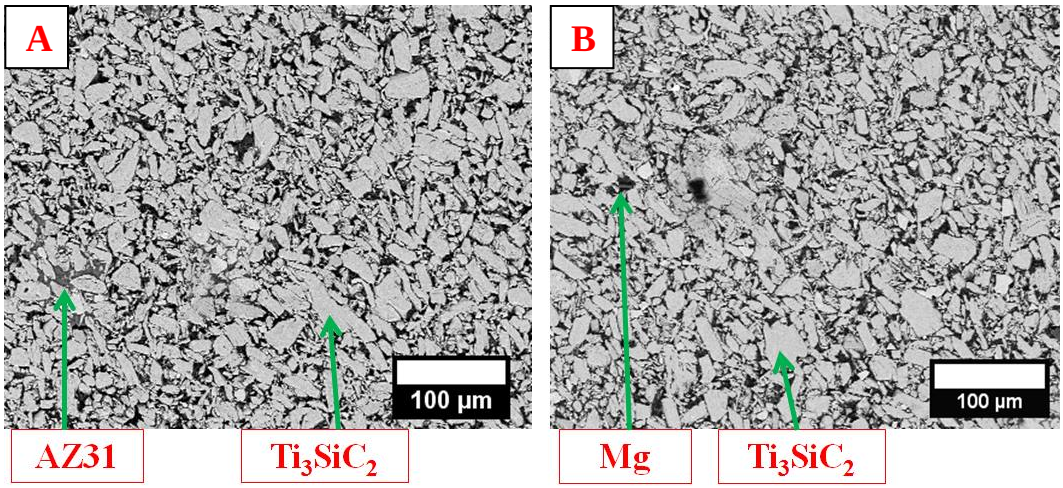

Figure 21: SE mode SEM images of Ti/55/31 (A) and Ti/55/Mg (B) composites displaying the MAX phase reinforcement and matrix materials.

Back scattered electron (BSE) mode images were taken of the Ti/55/Mg and Ti/53/61 composites (Fig. 22). The images display distinct areas where the matrix component has not been pulled out. Both images display a severely kinked and delaminated MAX phase grain microstructure.

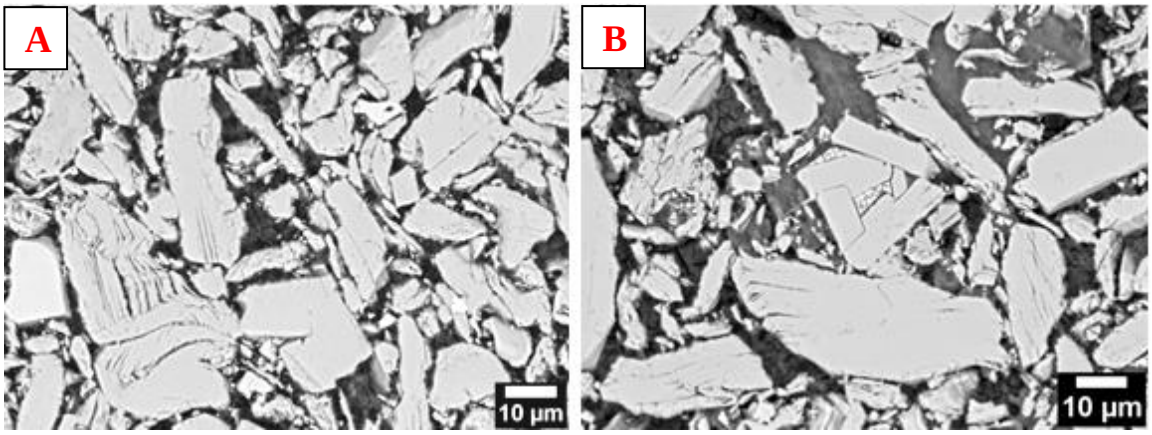

Figure 22: SEM images of Ti/55/Mg (A) and Ti/53/61 (B) composites revealing intact matrix components and a severely kinked and delaminated microstructure.

An energy dispersive spectroscopy (EDS) line scan of 31 points spanning approximately 3 µm across a Ti/55/Mg composite interface was performed. The purpose of this was to characterize the existence of penetrated Mg into Ti_3SiC_2 microcracks and nanofissures; a consequence of the melt infiltration process (Fig. 23). At approximately 1.5 µm, or directly in the center of the scan and in the center of a nanofissure, the existence of Mg was confirmed by the spike in atomic composition (Fig. 23).

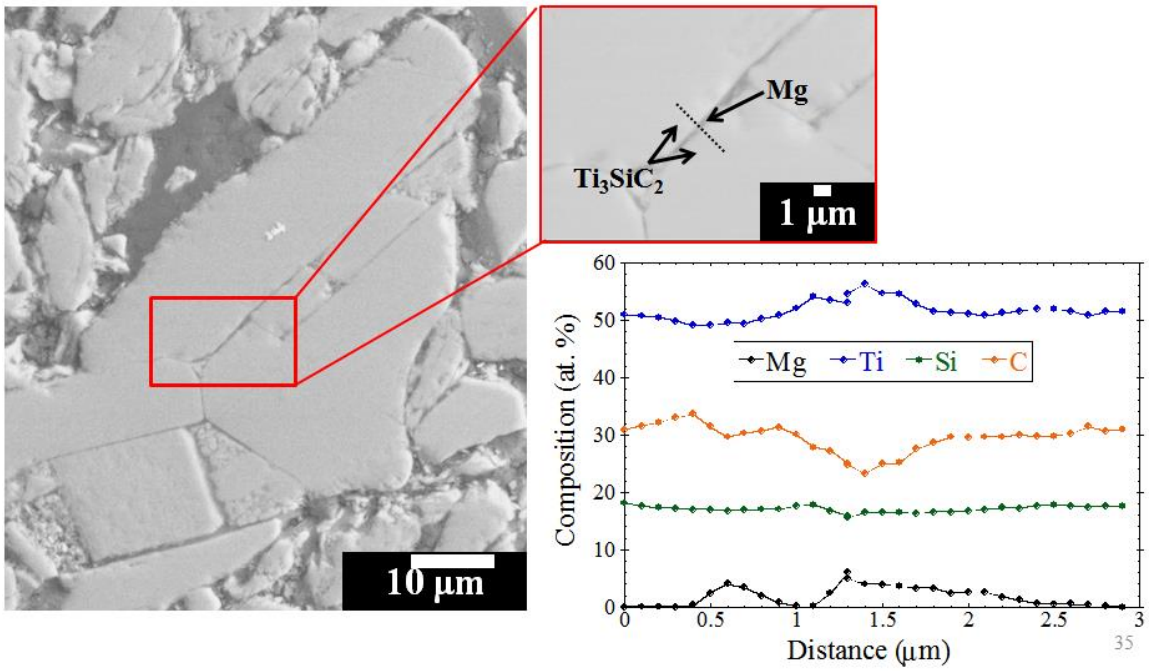

Figure 23: EDS line scan confirming the presence of penetrated Mg into a Ti_3SiC_2 grain nanofissure.

The pre-stressed microstructure and morphology of the Cr_2AlC grains was found to be un-kinked, not delaminated and circular (Fig. 24).

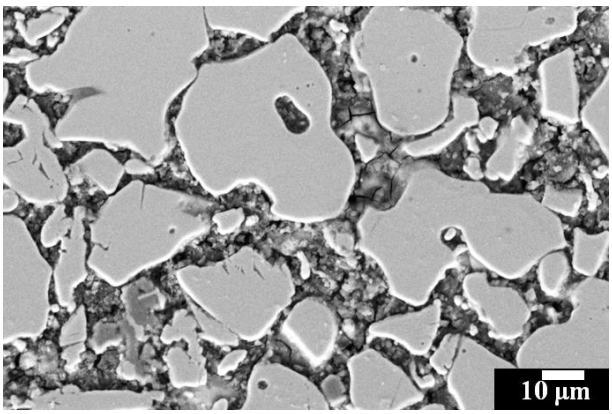

Figure 24: Cr_2AlC un-kinked and non-delaminated circular microstructure and morphology.

The National Institute of Health's free image analysis software, ImageJ, was used for grain size analysis. The analysis was performed on polished composite surfaces using the linear intercept method as described by ASTM E112-10. Thirty five measurements were made on Ti_3SiC_2 and Cr_2AlC grains. Average grain sizes of 10.8 ± 8 and 10.6 ± 7 were found for the Ti_3SiC_2 and Cr_2AlC MAX phase reinforcements, respectively.

5.5 Vickers Microhardness

Vickers microhardness results were gathered for each of the Ti_3SiC_2/Mg-alloy and Cr_2AlC/Mg-alloy composites. The respective results were compared with previous work on Ti_2AlC/Mg-alloy composites (Fig. 25).[26] The maximum hardness was found with MAX phase reinforcements melt infiltrated with AZ91. Ti_2AlC/AZ91, Ti/55/91 and Cr/55/91 were found to have a maximum hardness of 2.2 ± 0.1, 1.9 ± 0.1, and 1.5 ± 0.1 GPa, respectively. It was observed that the Ti_3SiC_2 MMC's have an increasing trend in hardness with additions of Al wt. % content in the matrix. However, Cr_2AlC MMC's exhibit an initial drop then subsequent rise in hardness with each addition of Al wt. % content in the matrix.

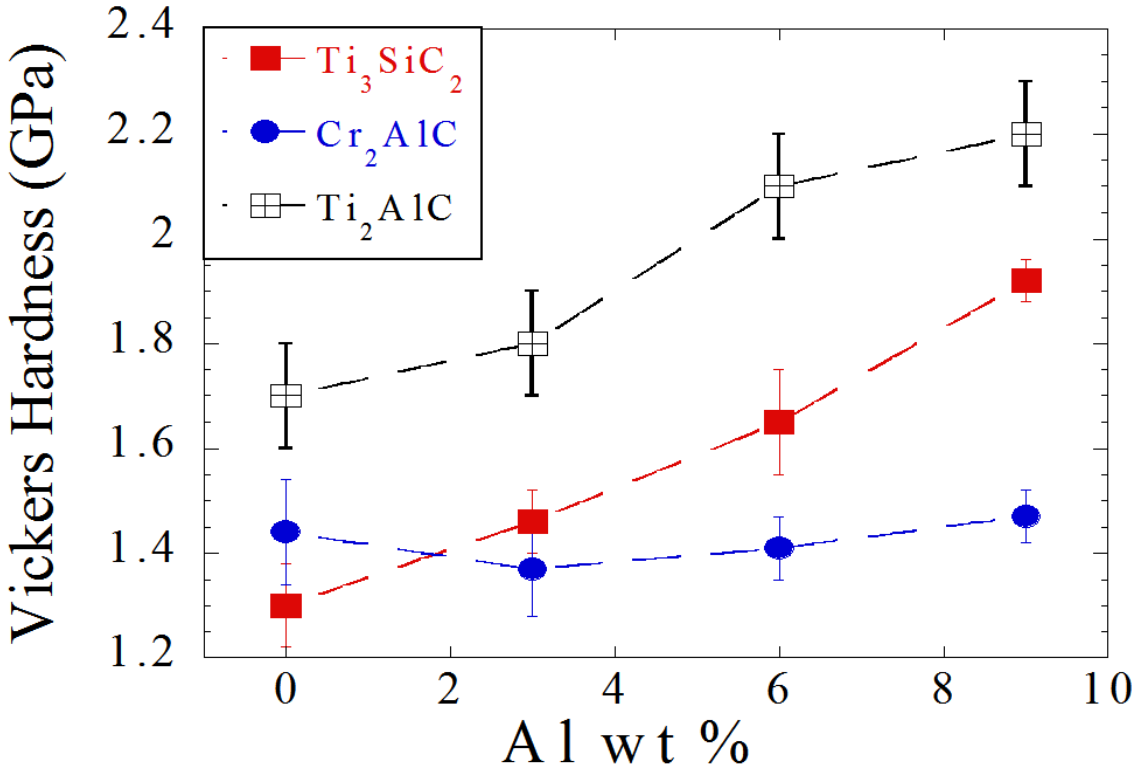

Figure 25: Vickers microhardness results vs. matrix Al wt. % content for each composite in this work compared with previous work on Ti_2AlC/Mg [26] composites.

5.6 Ultimate Compression Strength

Five 4 mm^3 samples were crushed to obtain five UCS values for each composite. Those five values were averaged with standard deviations found to generate UCS data for each of the Ti_3SiC/Mg and Cr_2AlC/Mg composites. The respective results were compared with previous work on Ti_2AlC/Mg-alloy composites (Fig. 26).[26] Ti_2AlC/AZ31, Ti/55/91 and Cr/55/91 were found to have a maximum UCS of 773±7, 617±10, and 545±35 GPa, respectively. The Ti_3SiC_2 reinforced MMC's generally show an increasing trend in UCS with each addition of Al wt. % in the matrix. The Cr_2AlC reinforced MMC's exhibit an

initial drop, then subsequent rise in UCS with each addition of Al wt. % content in the matrix.

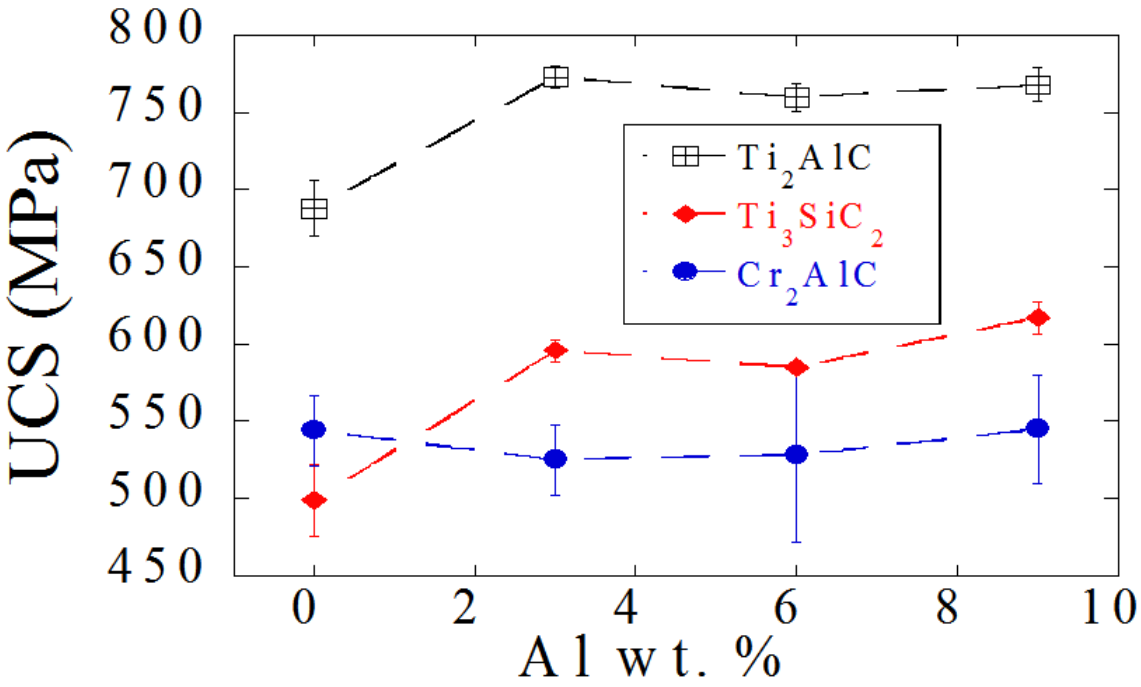

Figure 26: Comparison of UCS testing results vs. Al wt. % content for in for each composite in this work compared with previous work on Ti_2AlC/Mg [26] composites.

5.7 Elastic Moduli

Effective moduli were plotted as a function of cyclic compressive stress (Fig. 27). Each effective modulus data point was extracted from the slope of its respective hysteresis loop. The hysteresis loops were the result of the ~ 65% of maximum UCS cyclic compression testing.

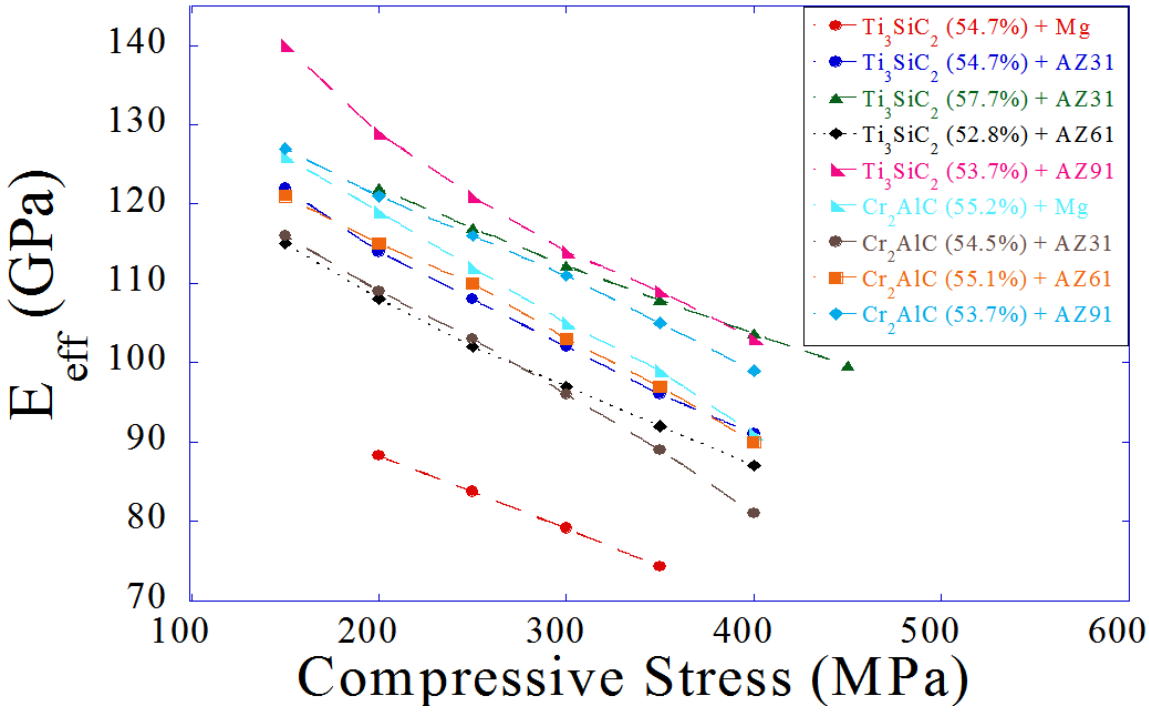

Figure 27: Effective moduli vs. compressive stress for every composite in this work.

Narrowing down the composites, a comparison was made between the Ti/55/Mg, Ti/55/31, Ti/58/31 and Ti/54/91 effective moduli vs. compressive stress (Fig. 28). The purpose of this was to showcase the effect, from small changes in Ti_3SiC_2 preform volume % density, in the Ti/55/31 and Ti/58/31 composites fabricated with AZ31. The two composites were processed and synthesized from identical batches of materials. The Ti/55/31 and Ti/58/31 effective moduli at a compressive stress of 200 MPa were found to be 114 and 122 GPa, respectively. Thus, a 3% increase in preform density increased the effective modulus of the composite by 7 GPa, equating to a 6% increase. Interestingly, a non-linear increase is observed in the Ti/54/91 effective moduli at low stresses whereas all the other composites in this work display an approximate linear change in the effective

modulus with applied compressive stress. At higher stresses, it was observed that the effective modulus of the Ti/58/31 composite rivaled that of the Ti/54/91 composite.

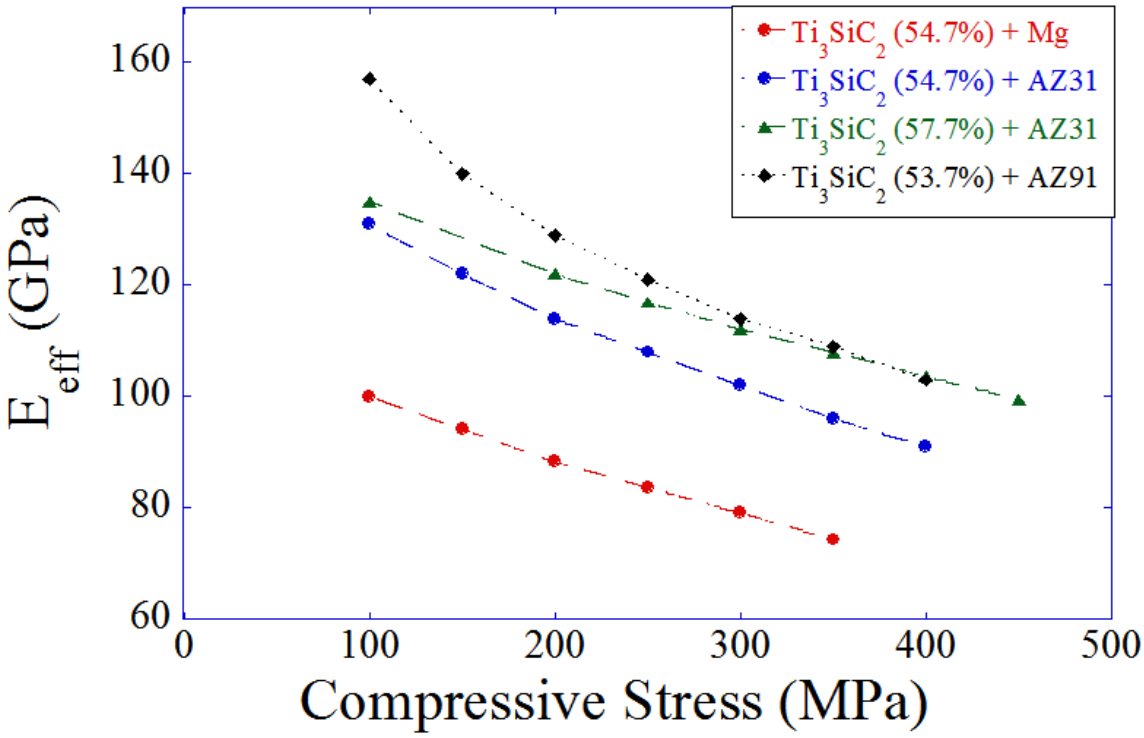

Figure 28: The effect of small changes in MAX carbide preform volume % density (blue vs. green curves) directly increases mechanical properties.

Prior work on Ti_2AlC/Mg [26] and this work on Ti_3SiC/Mg and Cr_2AlC/Mg-alloy composites have shown a maximum $E_{eff(avg)}$ of 114 ± 4, 125 ± 19 and 116 ± 12 GPa, respectively (Fig. 29). Both Ti_3SiC_2 and Cr_2AlC showed their highest effective modulus when melt infiltrated with AZ91. In comparison, Ti_2AlC melt infiltrated with AZ61 gave rise to its maximum $E_{eff(avg)}$.[26] It is observed that Ti_2AlC's effective modulus increases upon additions of 3 and 6 Al wt. % content in the matrix, and decreases from 6 to 9 Al

wt. %. Ti_3SiC_2 shows an increase in effective modulus upon additions of 3 and 9 Al wt. %, but a decrease from 3 to 6 Al wt. %. The Cr_2AlC/Mg composites' $E_{eff(avg)}$ show the same trends as witnessed in other mechanical tests: the data initially falls and then subsequently rises with each addition of Al wt. % content in the matrix.

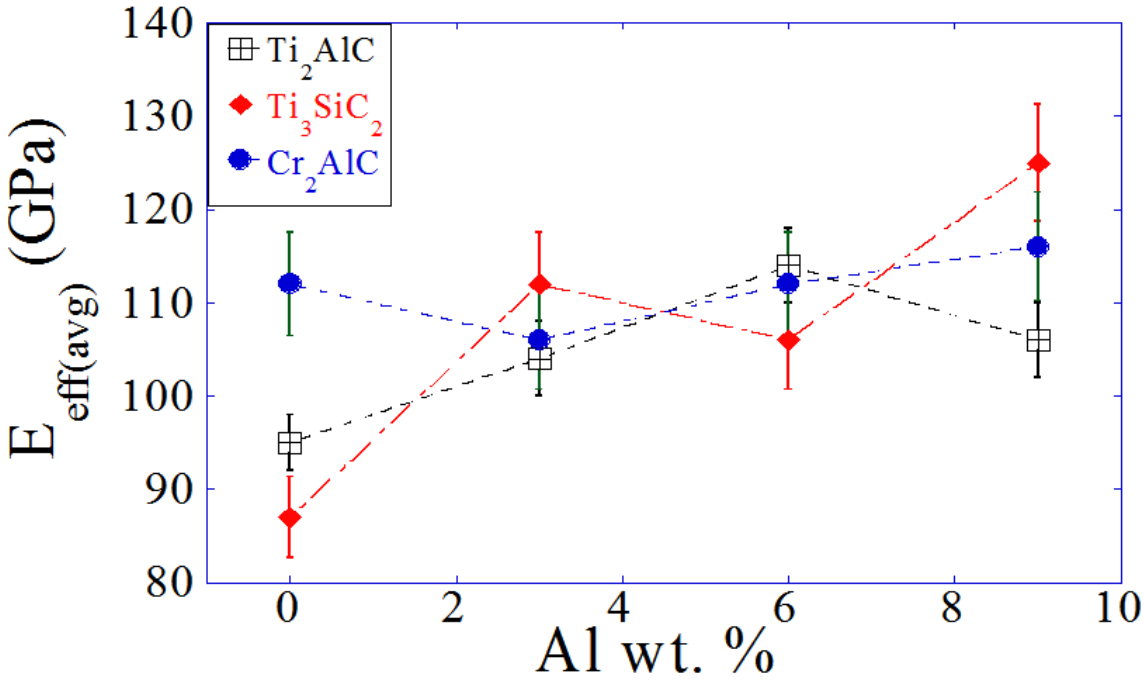

Figure 29: $E_{eff(avg)}$ as a function of Al wt. % content in the matrix for Ti_3SiC_2, Cr_2AlC and Ti_2AlC [26] MMCs.

$E_{100(avg)}$ values for Ti_3SiC_2/Mg, Cr_2AlC/Mg, and previously worked Ti_2AlC/Mg-alloy composites, were compared (Fig. 30). [26] The $E_{100(avg)}$ values are the best estimate to the true elastic modulus for these materials. The maximum $E_{100(avg)}$ for the Ti_2AlC/Mg, Ti_3SiC_2/Mg, and Cr_2AlC/Mg-alloy composites were found to be 136 ± 6, 159 ± 3 and

133±1 GPa, respectively. The same exact trends in mechanical properties for the $E_{eff(avg)}$ are witnessed in the $E_{100(avg)}$ data.

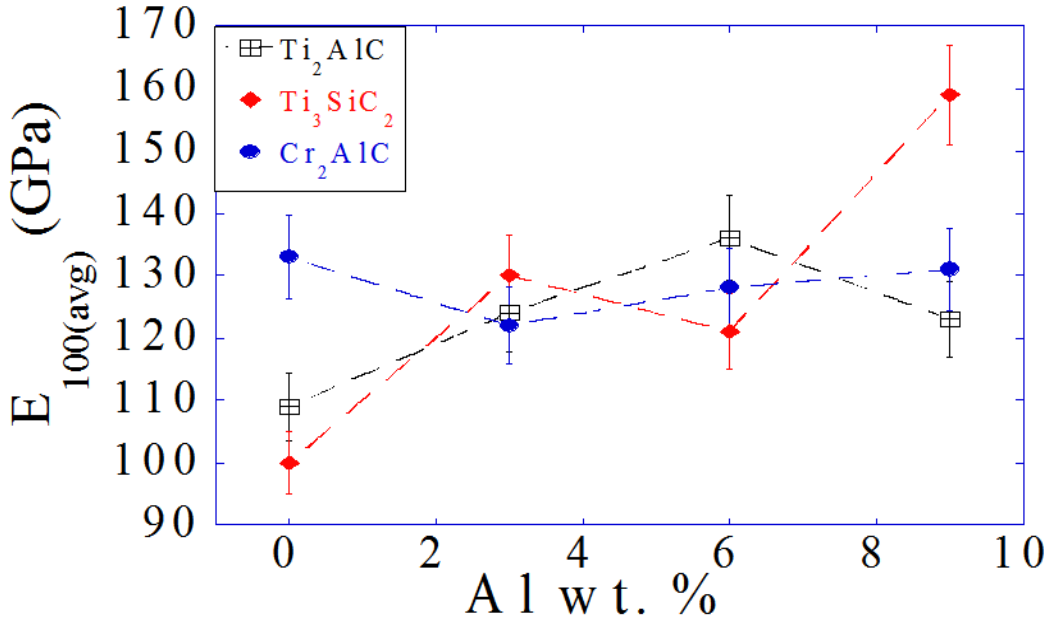

Figure 30: $E_{100(avg)}$ as a function of Al. wt. % content in the matrix for Ti_3SiC_2, Cr_2AlC and Ti_2AlC [26] MMCs.

5.8 Yield Strength

The maximum YS for the Ti_2AlC, Ti_3SiC and Cr_2AlC reinforced MMCs were found to be 426±54, 353±3, and 318±2 MPa, respectively (Fig. 31).[26] It was observed that both the Ti_2AlC and Ti_3SiC_2 MMCs have a generally increasing trend in YS with additions of aluminum wt.% content in the matrix, whereas Cr_2AlC MMCs exhibit the same initial drop and subsequent rise in YS; as characteristic with its behavior in relation to other mechanical strengths in this work.

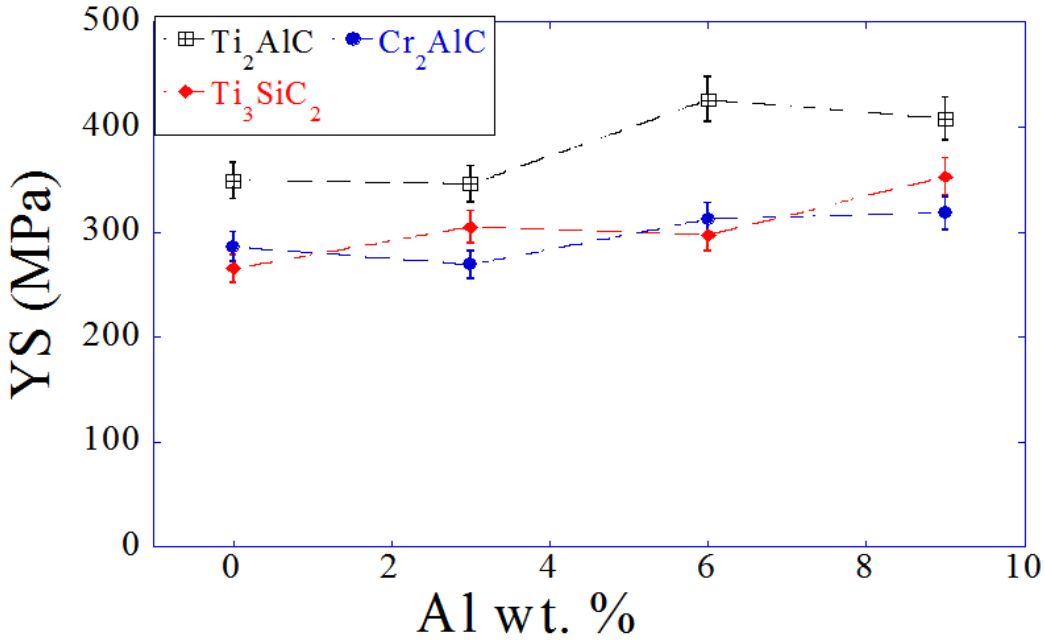

Figure 31: Yield strength as a function of Al wt. % content in the matrix of Ti_2AlC [26], Ti_3SiC_2 and Cr_2AlC MMC's.

5.9 Cyclic Compression Testing

Each Cr_2AlC/Mg and Ti_3SiC_2/Mg-alloy composite exhibited nested, closed, fully reversible hysteresis loops. These loops were extracted from their respective stress-strain curves and were subsequently re-plotted in a more aesthetically pleasing fashion (Figs. 32, 33). Re-plotting the loops in this manner does not change any data associated with their energy dissipative nature; it simply shifts the loops to the origin of the graph, making them more pleasing to the eye.

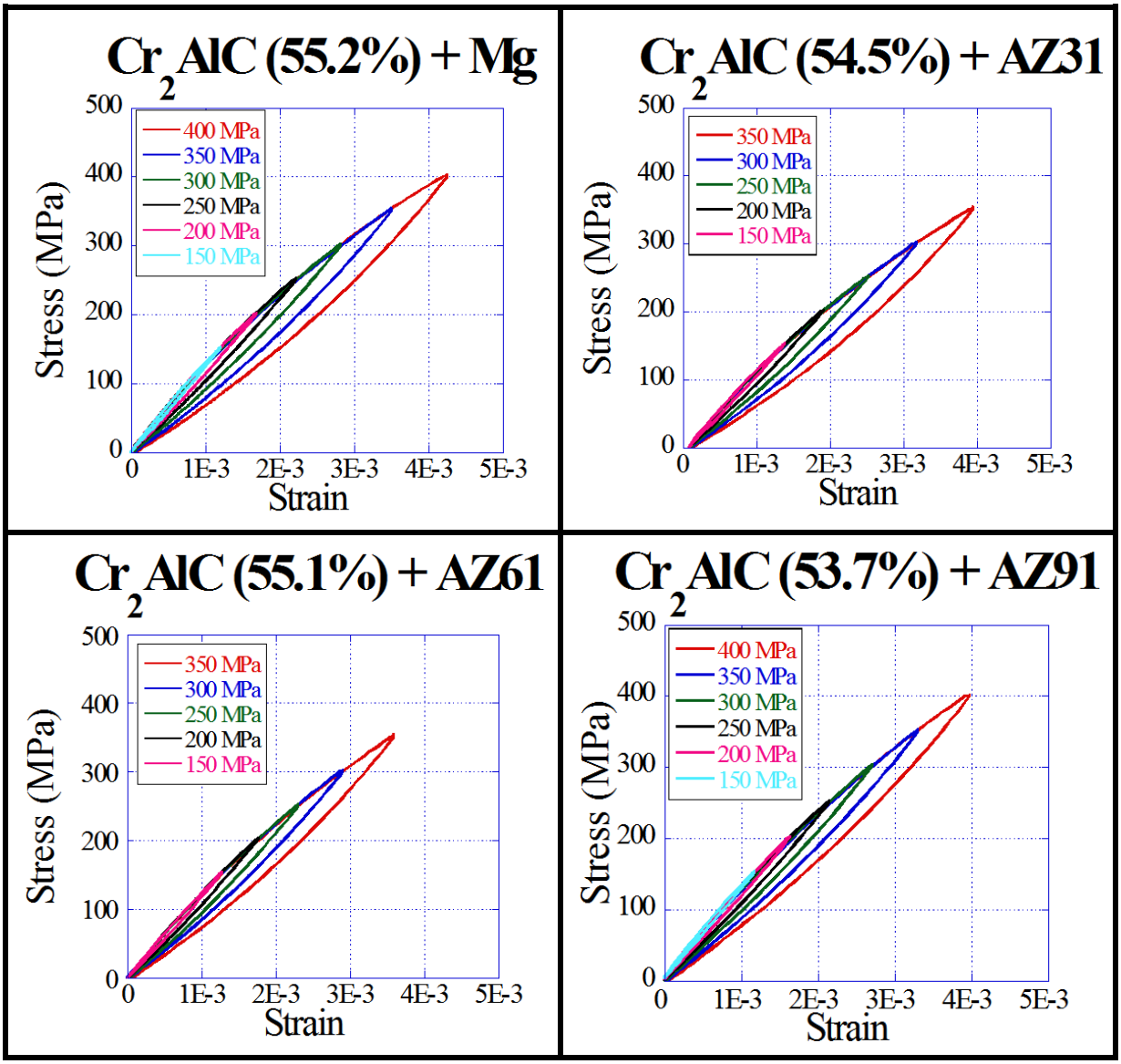

Figure 32: Cyclic compression testing results of Cr_2AlC reinforced MMCs displaying nested, closed, fully reversible energy dissipating loops.

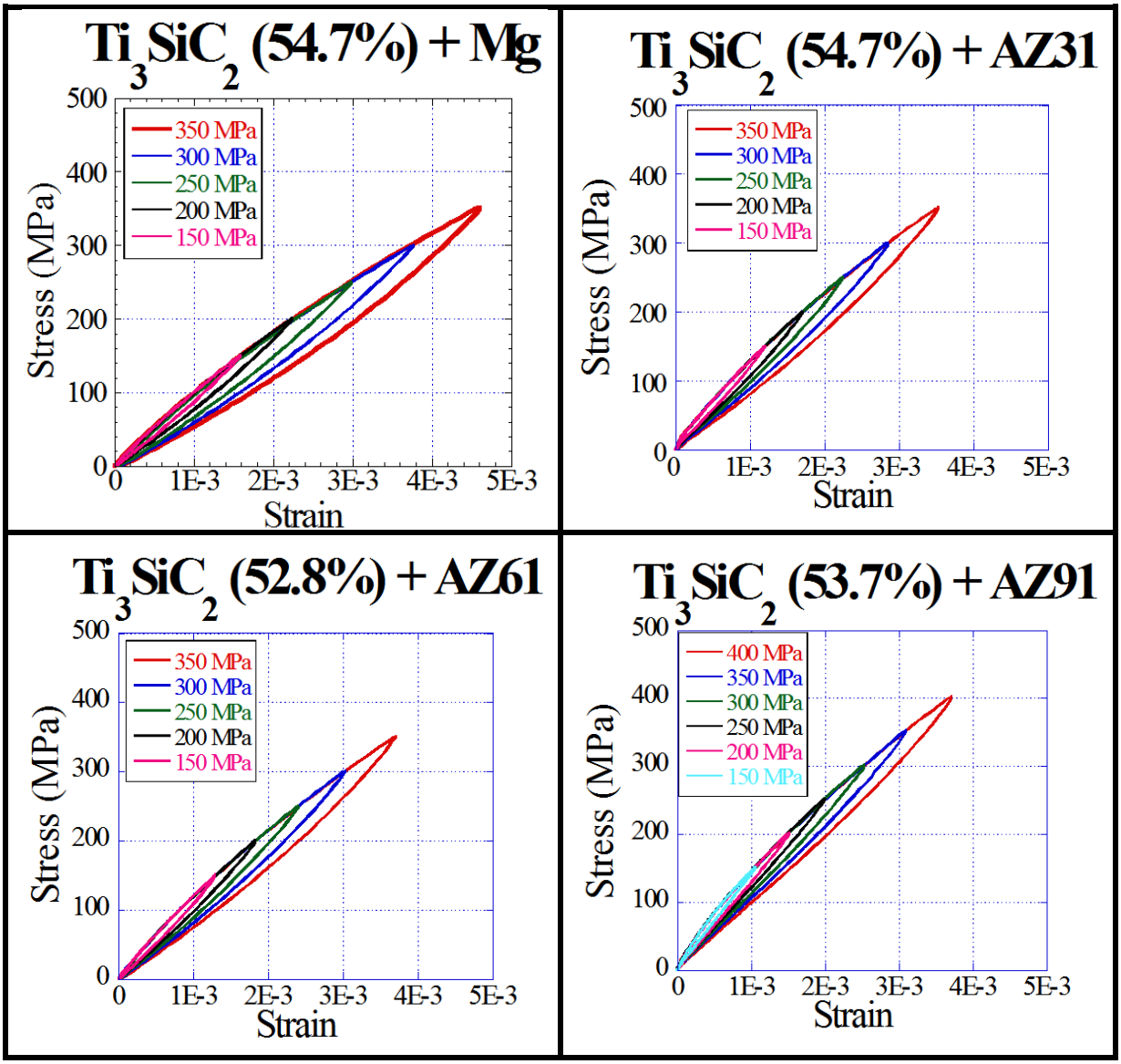

Figure 33: Cyclic compression testing results of Ti3SiC2 reinforced MMCs displaying nested, closed, fully reversible energy dissipating loops.

5.10 Effect of Preform Density on Mechanical Properties

The Ti/55/31 and Ti/58/31 composites were been compared in regards to every other mechanical test performed in this work (Table 2). The $E_{100(avg)}$, $E_{eff(avg)}$, YS, UCS and VH results for the Ti/55/31 and Ti/58/31 composites have been found to be 130±1 and 135±1 GPa, 112±13 and 115±12 GPa, 260±5 and 300±4 MPa, 596±7 and 639±17 MPa, and 1.46±0.1 and 1.63±0.1 GPa, respectively. The 3% increase in carbide preform volume % density produced 7%, 10% and 13% increases in UCS, VH and YS, respectively. This effect was substantial enough to allow the Ti/58/31 composite's UCS to surpass the Ti/54/91 composite's UCS.

Table 2: Comparison of MMC mechanical properties as a result of small changes in MAX phase preform density

Sample	$E_{100(avg)}$ (GPa)	$E_{eff(avg)}$ (GPa)	YS (MPa)	UCS (MPa)	VH (GPa)
Ti_3SiC_2 (54.7%) + AZ31	130 ± 1	112 ± 13	260 ± 5	596 ± 7	1.46 ± 0.1
Ti_3SiC_2 (57.7%) + AZ31	135 ± 1	115 ± 12	300 ± 4	639 ± 17	1.63 ± 0.1
Ti_3SiC_2 (53.7%) + AZ91	159 ± 3	125 ± 19	346 ± 4	617 ± 10	1.92 ± 0.1

5.11 Machinability

The MAX phase reinforced composites in this work were readily machinable as typical for MAX phase constituents.[34,39] These composites are electrically conductive, therefore EDM was used to produce all the samples necessary for the mechanical testing required for this work.

5.12 Post-stress Evaluation of Microstructure

A SE mode image of four microhardness indents, ranging from the top left to the bottom right, in the Ti/55/31 composite was captured (Fig. 34). Indentation topography, a homogenous MAX phase reinforcement landscape, and several areas of intact matrix components in the composite microstructure were identified.

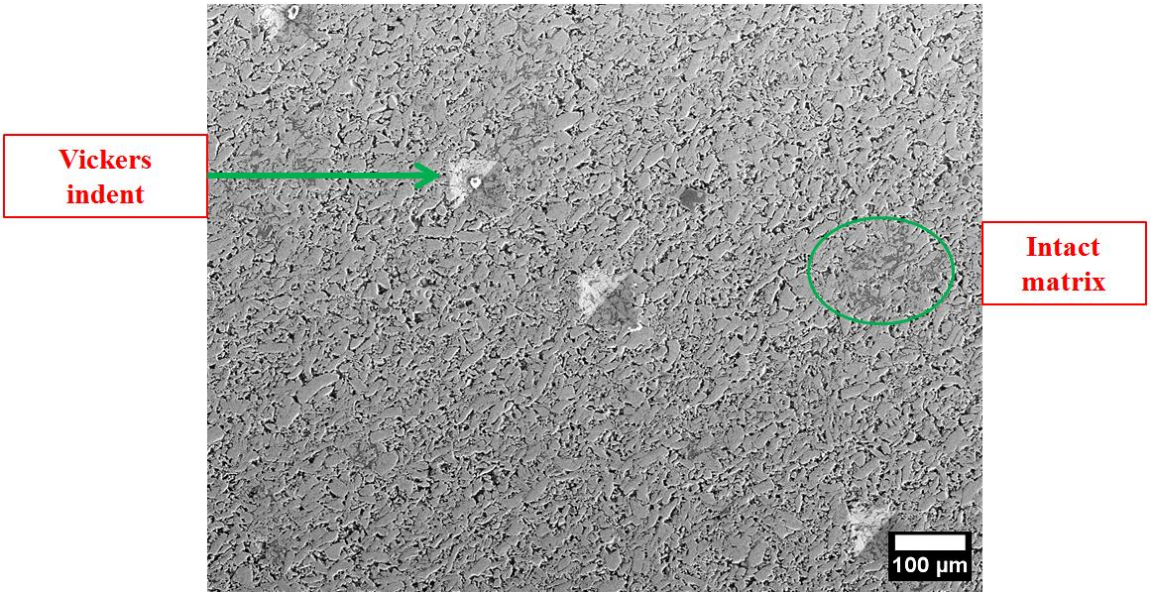

Figure 34: SE mode image of the Ti/55/31 composite displaying four microhardness indents, the homogenous MAX phase reinforcement landscape, and areas of intact matrix.

One indent was imaged from each of the Ti/54/31 and Ti/57/31 composites in SE mode (Fig. 35). There is a 3 volume % density difference between these two composites, both of which were MI with AZ31. The matrix phase was observed to be intact inside the

indent perimeter. Outside the indent perimeter, however, both composite microstructures display regions where the matrix material was pulled out.

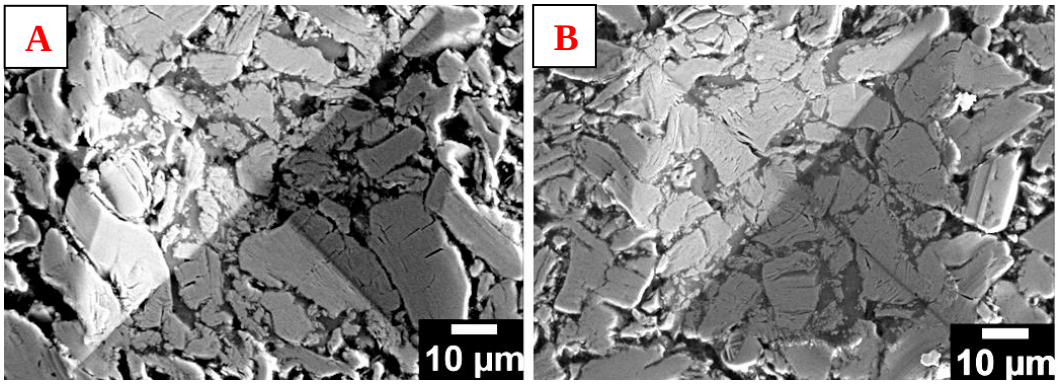

Figure 35: SE mode SEM images of microhardness indents in Ti/54/31 (A) and Ti/57/31 (B) composites revealing matrix areas outside the indent perimeter being pulled out, but intact within the indent itself.

SE and BSE SEM images were taken of a microhardness indent in the Cr/55/31 composite (Fig. 36). In the SE mode image, indent topography and pull-out areas outside the indent perimeter were identified. In the BSE image, z-contrast promoted easy distinction between the matrix and carbide reinforcement. The Cr/55/31 composite does not display kinked and delaminated grains, but the grains which received indentation do display microcracking. The polished surface shows the Cr_2AlC grains kept their circular morphology post-stress testing.

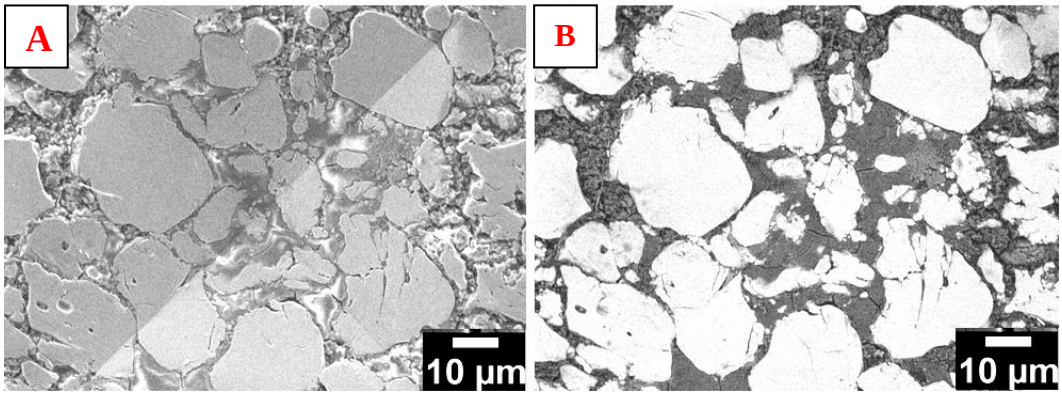

Figure 36: SE (A) and BSE mode (B) SEM images of a microhardness indent in the Cr/55/31 composite.

SEM was performed on polished surfaces of the Cr/55/31 composite UCS samples. The samples were mounted in hard epoxy in longitudinal (tensile) and transverse (compressive) directions to the applied compressive stress (Fig 37). The purpose of viewing the samples on these surfaces was to observe if the Cr_2AlC microstructure had become kinked and delaminated after being subjected to stress in different directions.

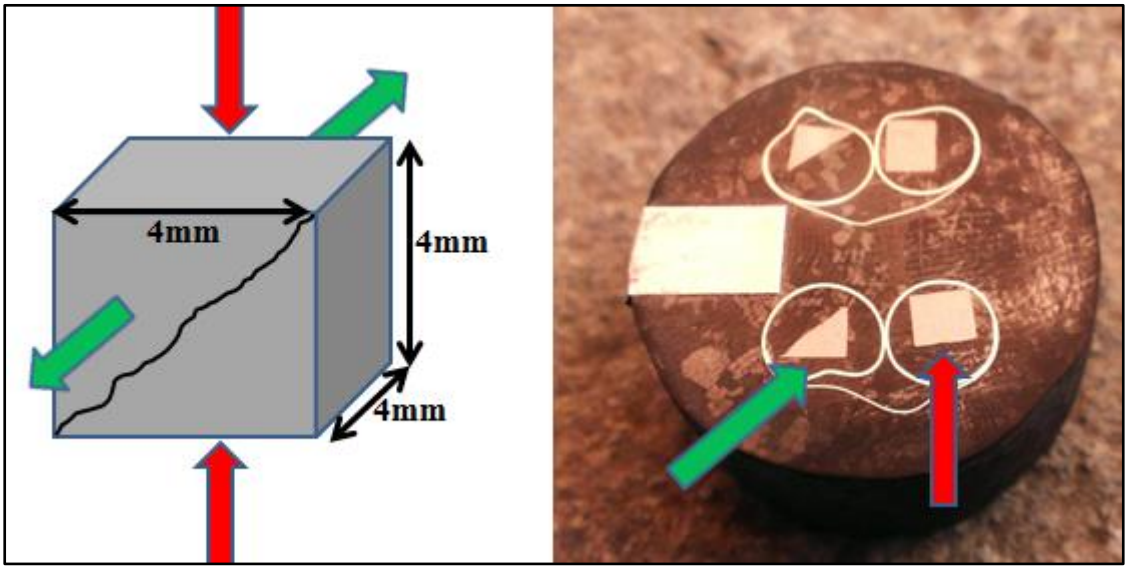

Figure 37: Schematic displaying directions transverse (red arrows) and longitudinal (green arrows) surfaces to the applied compressive stress direction (left). One longitudinal and one transverse stress direction UCS sample from each Ti_3SiC_2 (right: top) and Cr_2AlC reinforced composite (right: bottom).

A transverse section of the Cr/55/31 composite reveals a small volume fraction of kinked and delaminated grains (Fig. 38). There is clear evidence of matrix pull out, and it appears that no Mg-alloy has infiltrated to exist in the microcracks of the reinforcement phase. This suggests that these cracks formed after stressing the materials, or that AZ31 did not penetrate into the microcracks during melt infiltration.

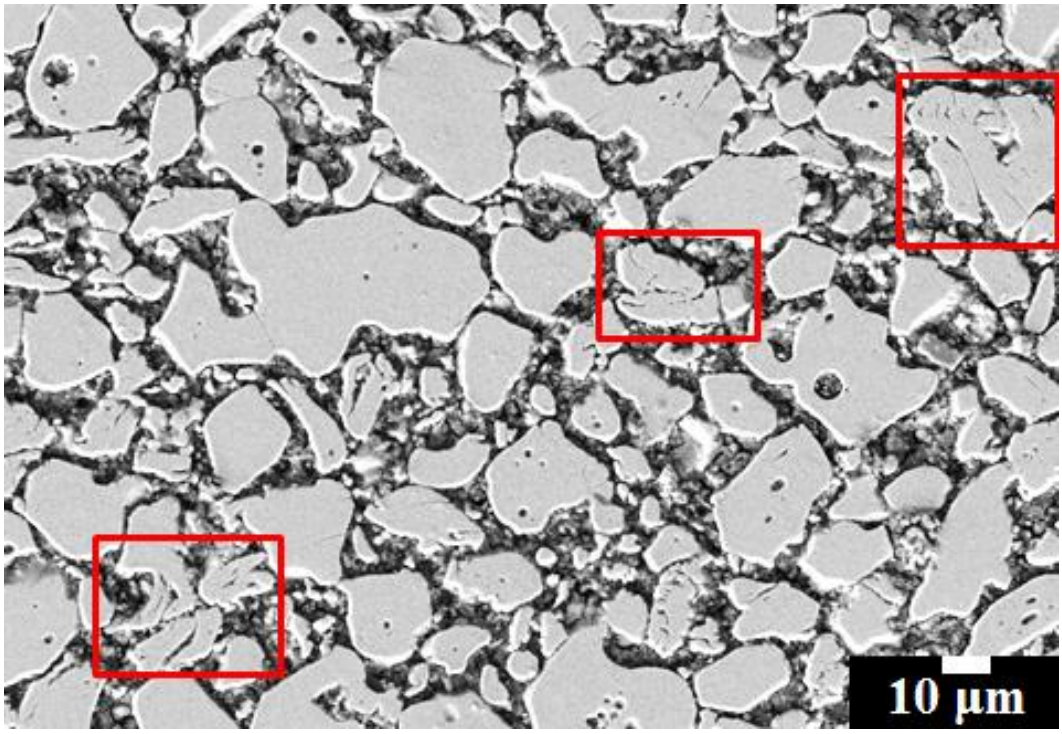

Figure 38: Kinked and delaminated Cr_2AlC grains in the transverse to stress direction sample of the Cr/55/31 composite.

Visual inspection had allowed the identification of different morphologies on the longitudinal (tensile) fracture surface edges for the Cr_2AlC/Mg and Ti_3SiC_2/Mg-alloy composites (Fig. 39). The fracture edge morphology for the Cr_2AlC/Mg and Ti_3SiC_2/Mg-alloy composites appeared to be curved and jagged, and linear and smooth, respectively.

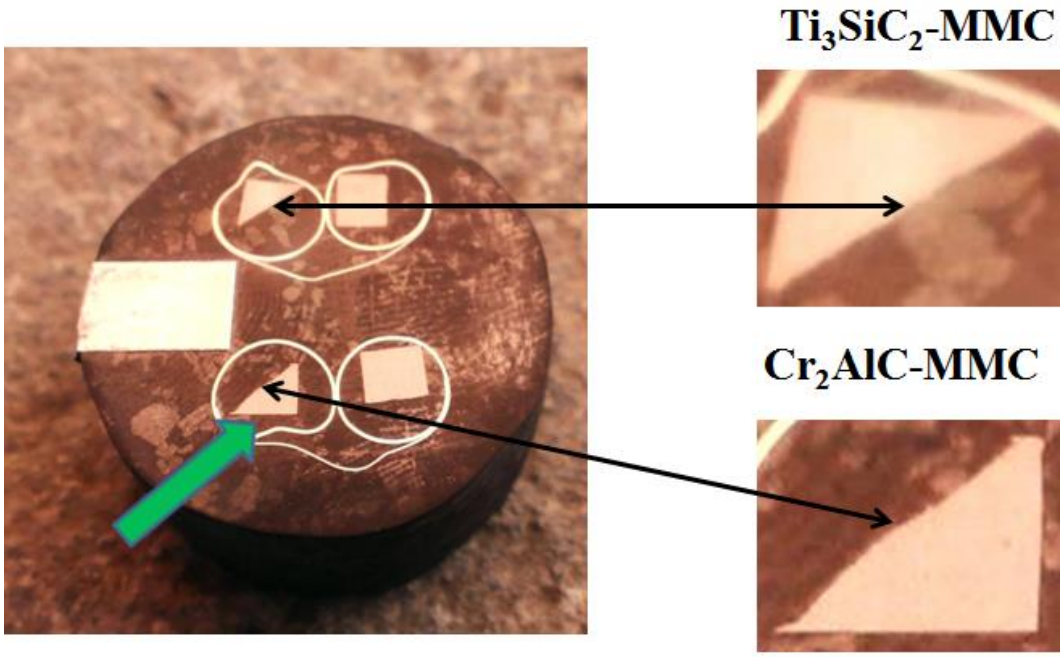

Figure 39: Visual inspection revealing differences in the longitudinal (tensile) fracture surface edge morphologies of the Ti and Cr based Mg-alloy composites.

These fracture morphologies were believed to be a direct result of the MAX phase grain microstructure and morphology. Therefore, these fracture surface edges of interest were studied using optical microscopy (Figs. 40, 41).

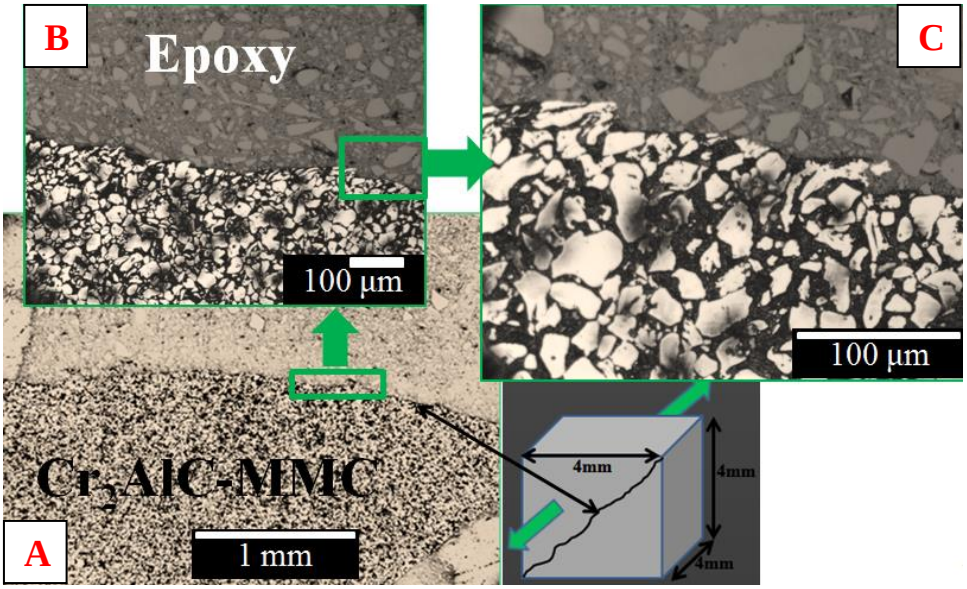

Figure 40: Curved fracture edge morphology of the Cr_2AlC based composite (A); a curved and jagged area of interest on the fracture edge (B); magnified area of interest displaying the curved and jagged fracture morphology (C).

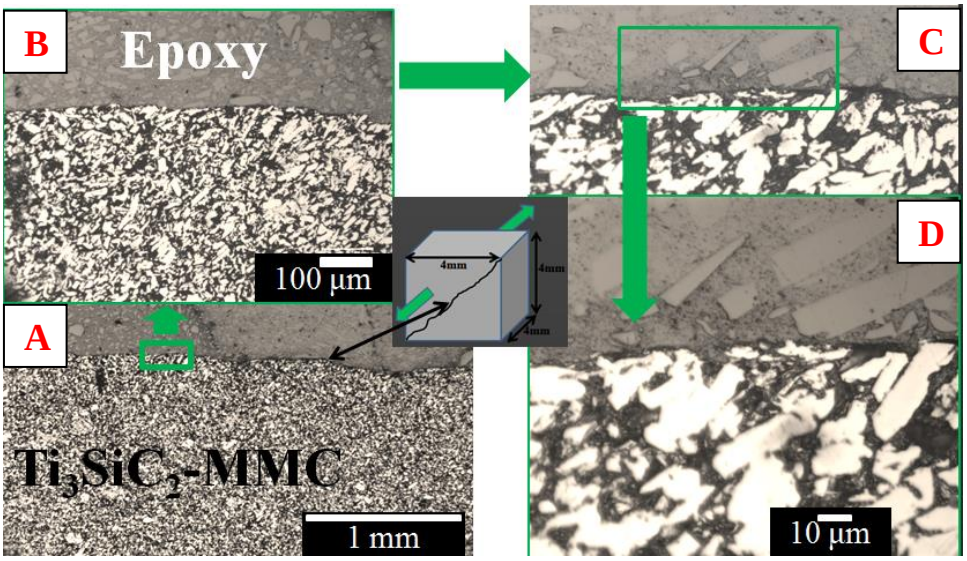

Figure 41: Linear and smooth fracture edge morphology of the Ti_3SiC_2 based composite (A); linear and smooth area of interest on the fracture edge (B); magnified areas of interest of the smooth linear fracture morphology (C, D).

6. Discussion

6.1 XRD

Bulk sections were taken from the composites for all the XRD experiments barring one exception: the in-house synthesized Cr_2AlC powder. Bulk samples were used rather milling portions of the composites into powder. Milling physically deforms the powder; inducing unwanted strain into the Mg and Mg-alloy grains. Additionally, by scanning a bulk sample, the composite interface was hoped to be preserved, whereas milling into fine powder may destroy any long-range interfaces.

Post-annealed XRD results for the Cr/55/Mg composite did not show any reaction phases as a result of annealing. The comparison of pre and post-annealed spectra does show a reduction in the Cr_2AlC/Mg main peak intensity at ~ 42° 2-theta and a slight reduction in all the other Cr2AlC/Mg peaks (Fig. 18). The exact nature for why this has occurred is unclear. The most reasonable explanation for this is that the pre and post-annealed parallel plate XRD samples not were not identically parallel.

Two observations were made from the XRD results after annealing the Ti/55/Mg composite: 1) the large peak at ~10° 2-θ associated with Ti_3SiC_2 had reduced intensity and 2) the intensity of the Mg_2Si peak at ~ 24° 2-theta decreased slightly (Fig. 19). This is most likely, again, due to the parallel plate samples not being perfectly parallel. No reaction phases were identified as a result of annealing.

In comparison to the pre-annealed condition of the Ti/55/Mg composite, the Ti/54/91 shows a less intense peak at ~ 10° 2-θ associated with Ti_3SiC_2 (Fig. 20). On the other hand the Mg_2Si peak at ~ 24° 2-theta appears to have increased when comparing these two composites. Since no reaction phases were seen after annealing in this composite, an appropriate explanation for the changes in peak intensity is indeed the thin cross sectioned parallel plates not being exactly parallel.

It was initially hypothesized that Mg_2Si would be found as a product of the reaction during the melt infiltration processing step. XRD has proven the existence of Mg_2Si in the Ti_3SiC_2/Mg-alloy composites. As previously discussed, Mg_2Si has been shown to be present in composites due to a reaction between SiC and Mg.[19,20] The true effect of this reaction product on composite mechanical properties is unclear, however, it is observed that Mg_2Si does not inhibit an increase in mechanical properties for the Ti_3SiC_2 reinforced MMCs.

Overall, none of the annealed composite samples displayed any reaction phases when comparing XRD spectra of the pre and post-annealed condition. This suggests that, to a certain limit, these composites are suitable for elevated temperature usage. Applying these composites to elevated temperature environments would require further mechanical testing to understand other strength limitations before use.

6.2 Trends in Mechanical Properties

This work on Ti_3SiC_2/Mg and previous work on Ti_2AlC/Mg composites both show trends of increasing mechanical properties with increases of Al wt. % content in the

matrix. It is believed that aluminum plays a strong role to enhance the matrix-to-reinforcement interface.[24,26] The absence of Al in the Ti/55/Mg composite suggests a weaker interface than Ti_3SiC_2/Mg composites infiltrated with AZ31, AZ61 and AZ91. This trend can be observed in the Ti_3SiC_2/Mg-alloy mechanical properties reported in the results section.

The trend of increasing mechanical properties with increasing Al wt. % content is not observed with the Cr_2AlC based composites. An initial reduction in mechanical properties is consistently observed for the Cr_2AlC/Mg-alloy composites. Upon the first contribution of Al, from pure Mg to AZ31, the mechanical strengths decrease. Increases in the Al wt. % content in the matrix produced a small consistent rise in Cr_2AlC MMC mechanical strengths. Only when Cr_2AlC was melt infiltrated with AZ91 were the mechanical strengths either comparable to, or better than, those of Cr_2AlC melt infiltrated with pure Mg.

The trends in mechanical strengths of the Cr_2AlC based composites suggest that one of the constituents from the AZ series alloys has a deleterious effect on the matrix-reinforcement interface. The hypothesis is that the interface is being weakened upon melt infiltration via AZ alloys. Moving from AZ31 to larger amounts of Al wt. %'s in 3% increments (AZ61 & AZ91) is consistently coupled with linearly increasing mechanical strengths. Therefore it is suspected that the mechanical properties are being increased due to solid solution strengthening by Al within the Mg-alloy grains. Since linear increases in strengths are believed to be the result of increasing the Al wt. % content, Zn is believed to be weakening the interface. This mechanical weakening is observed in all the

mechanical testing data when comparing the Cr_2AlC/Mg and Cr_2AlC/AZ31 composites (Figs. 25, 26, 29-31).

The Ti/54/91 composite was found to have the highest mechanical strengths in this work. Al's affinity to wet Ti, coupled with Mg's ability to infiltrate between the micro and nanofissures of kinked and delaminated MAX particles may be the sole explanation for the high mechanical properties witnessed in the Ti_3SiC_2/Mg-alloy composites.

Microscopy images of Cr_2AlC reinforcement grains did not have an abundant amount of kinking and delamination (Figs. 24, 36, 38, 40). This provides two strong points of argument for the reduced mechanical properties observed for the Cr_2AlC/Mg-alloy composite system: 1) Mg or Mg-alloys did not have opportunity to penetrate between Cr_2AlC particle microcracks and nanofissures to create the strong mechanical interlocking witnessed in the Ti_3SiC_2 based composite system and; 2) Al may not wet the Cr surface as well as it does with Ti. These two reasons, especially the first, may provide fundamental insight into understanding physical mechanisms between the matrix and reinforcement phases which creates the strong mechanical interlocking responsible for resulting in MMCs with excellent mechanical properties. It is suspected that if the Cr_2AlC grains were kinked and delaminated, pure Mg and the AZ alloys would have penetrated between the microcracks and nanofissures. If this was to occur, it is hypothesized the mechanical strengths for the Cr_2AlC/Mg-alloys would increase, causing an upward shift of each line on each graph (Figs. 25, 26, 29-31). The trends in

the data would, however, not be affected and would remain the same due to the deleterious effect of AZ alloy constituents on the matrix interface.

6.3 Energy Dissipation

Upon cyclic compression testing, nested and fully reversible hysteretic stress-strain loops were seen for every MMC fabricated in this work. These results are identical to previous with work on Ti_3SiC_2.[42] It has been shown that the dissipated energy per unit volume per cycle, W_d, increases as the square of the maximum applied stress: $W_d \propto \sigma^2$.

Incipient kink bands (IKB) are the micromechanism responsible for the behavior seen in the cyclic compression tests[42] (Figs. 32, 33). The energy dissipative behavior witnessed in these materials, and other MAX phase based composites, can be explained by IKB mechanisms. IKB mechanisms have given rise to label materials such as these as kinking non-linear elastic solids.[42]

The potential for dislocation loops isolated to the basal planes exits everywhere in these materials. Upon receiving stress, these dislocations loops emerge from the basal planes containing dislocations with opposite signs. When the material is stressed, the dislocation loops move away from each other and cause the loop to grow or expand. Upon stress relaxation, the dislocation loops move back together and annihilate. This process of growing and annihilating dislocation loops occurs during every cycle and this is what allows the reversible plastic deformation known as non-linear elastic deformation.

The cyclic hysteresis behavior that has been observed in these materials, and others [26,42], is promoted by the damping capability of the Mg-alloys and the MAX phase

reinforcements. The AZ series alloys, as well as other magnesium based alloys are observed to have very good damping capability. Some alloys have better specific damping capacity than others; AZ91 is one such alloy. AZ91D has an increasing specific damping capacity in respect to increasing stress: at 7, 14, 20, 25 and 30 MPa, the damping capacities are 2.67, 5.33, 12.0, 16.0 and 29.33%, respectively.[44] It is unclear if there is an upper bound to the increasing specific damping capability of the AZ alloys with applied stress. Nonetheless, this behavior suggests increased energy dissipation at higher stresses.

6.4 MAX Phase Microstructure and Morphology on Fracture

Fracture edge surfaces of Cr_2AlC and Ti_3SiC_2 composites were observed and compared using optical microscopy (Figs. 40, 41). Fracture edges for Cr_2AlC reinforced composites were shown to be wavy with jagged features at higher magnification. Fracture edges for Ti_3SiC_2 reinforced composites were shown to be straight with smooth features at higher magnification. The fracture edges in both composites can be described entirely by the reinforcement grain microstructure and morphology.

In regards to the Cr_2AlC reinforced composites, the wavy fracture edge appears to be due to the circular grain morphology. The jagged features on the fracture edge can be explained the lack of a kinked and delaminated microstructure: the propagating crack front is, for the majority of the time, forced to travel around the reinforcement grains. This gives rise to the propagating crack front leaving a jagged fracture edge.

In regards to the Ti_3SiC_2 reinforced composites, the straight fracture edge is most reasonably due to the elongated and rectangular shaped grain morphology. It is believed that the propagating cracked front can force these kinked and delaminated grains to shear and fracture off, leaving a straight smooth fracture edge behind.

7. Summary and Conclusions

MAX phase reinforced MMCs have been synthesized using Cr_2AlC and Ti_3SiC_2 preform reinforcements melt infiltrated with Mg and Mg-alloys. Mg and Mg-alloy composites were reinforced with 55±1 and 54±1 vol. % dense preforms of Cr_2AlC and Ti_3SiC_2, respectively. Microstructural and mechanical properties of these composites were explored and it has been concluded that:

1) Aluminum containing Mg-alloys show enhances mechanical strengths for Ti_3SiC_2 reinforced composites. Specifically, the Ti/54/91 composite displayed the highest properties in every mechanical test in this work. In contrast, the Ti/55/Mg composite had the lowest mechanical properties of the Ti_3SiC_2/Mg composites.
2) The VH, UCS, $E_{eff(avg)}$, $E_{100(avg)}$, and YS testing results do not display substantial increases in mechanical strengths from the addition of Al wt. % content in the matrix of $C_{r2}AlC$ reinforced composites. It is hypothesized that Zn from the AZ alloys is giving rise to a deleterious effect on the composite interface, causing an initial drop in mechanical properties when comparing Cr_2AlC composites with pure Mg and AZ31.
3) Nested, closed, fully reversible hysteresis loops were observed for every sample fabricated in this work. These loops are representative of the damping capability of Mg-alloys and the KNE solid behavior inherent to the MAX phases. Interestingly, without having a microstructure dominated by kinked and delaminated grains, cyclic hysteresis behavior persisted in the Cr_2AlC reinforced MMC's. Therefore, the nested,

cyclic hysteric nature exhibited by these composites has a damping component which stems solely from physical behavior inherent to the MAX crystallographic structure regardless if a kinked microstructure is present.

4) Microstructural characterization by SEM has made it clear that the Ti_3SiC_2 reinforcement phase is severely kinked and delaminated with an elongated rectangular morphology (Figs. 22, 33, 35). SEM imaging of Cr_2AlC/Mg-alloy composite polished surfaces did not show, pre or post-compressive stress testing, a microstructure dominated by kinked or delaminated grains (Figs. 24, 36, 38). SEM of Cr_2AlC grains depicts a circular morphology (Fig. 24, 36, 38).
5) The lower mechanical strengths of the Cr_2AlC reinforced composites are likely due to the Cr_2AlC grains not being kinked and delaminated. This will prevent Mg or AZ alloys from infiltrating microcracks and nanofissures. Aluminum's wettability on the chromium surface is questionable in its relationship to the mechanical strengths. A non-kinked MAX microstructure and a reduction in wettability are both points of evidence which can cause a reduction in mechanical properties.
6) The mechanical properties of the $C_{r2}AlC$/Mg and Ti_3Si_{C2}/Mg composites from this work have been summarized and compared to previous work on Ti_2AlC/Mg composites (Table 3).

Table 3: Summary of measured mechanical properties compared to previous work on Ti_2AlC MMC's.

MMC	$E_{100(avg)}$ (GPa)	$E_{eff(avg)}$ (GPa)	YS (MPa)	UCS (MPa)	VH (GPa)
Ti_2AlC/Mg	109 ± 4	95 ± 3	349 ± 3	688 ± 18	1.7 ± 0.1
Ti_2AlC/AZ31	124 ± 4	104 ± 4	346 ± 4	773 ± 7	1.8 ± 0.1
Ti_2AlC/AZ61	136 ± 6	114 ± 4	426 ± 5	760 ± 9	2.1 ± 0.1
Ti_2AlC/AZ91	123 ± 5	106 ± 4	408 ± 4	768 ± 11	2.2 ± 0.1
Ti/55/Mg	100 ± 1	87 ± 10	265 ± 1	500 ± 23	1.3 ± 0.1
Ti/55/31	130 ± 1	112 ±13	305 ± 1	596 ± 7	1.5 ± 0.1
Ti/53/61	121 ± 2	106 ± 11	297 ± 3	585 ± 3	1.7 ± 0.1
Ti/54/91	159 ± 3	125 ± 19	353 ± 3	617 ± 10	1.9 ± 0.1
Cr/55/Mg	133 ± 1	112 ± 15	286 ± 1	544 ± 23	1.4 ± 0.1
Cr/55/31	122 ± 2	106 ± 13	269 ± 1	525 ± 23	1.4 ± 0.1
Cr/55/61	128 ± 2	112 ± 11	312 ± 2	528 ± 56	1.4 ± 0.1
Cr/54/91	131 ± 4	116 ± 12	318 ± 2	545 ± 35	1.5 ± 0.1

8. Future Work

8.1 Effect of Preform Density on Mechanical Properties

The difference in mechanical properties between the two Ti_3SiC_2/AZ31 composites stemming from the vol. % density of the porous Ti_3SiC_2 sintered preforms is considerable. The effect of a small change in preform density (+3%) shows a considerable increase in mechanical properties. A full evaluation of mechanical properties for the two Ti_3SiC_2/AZ31 MMCs also compared with the Ti/54/91 composite which had the highest mechanical properties in this work (Table 2).

Although there was only a 3% increase in the effective modulus at 200 MPa, there are large increases in the VH, YS and UCS. Therefore it is suggested that future work investigating the mechanical properties with 60 vol.% reinforcement and 40 vol.% matrix composites should be investigated; especially for the work involving Ti_2AlC/AZ91 and TiC/AZ91 composites.

8.2 Mg_2Si

It is thought that the Mg_2Si reactant product creates a bonded Ti_3SiC_2 reinforcement and Mg matrix interface. If this is true, it may serve as the primary reason for observing the low mechanical strengths seen in the Ti_3SiC_2/pure-Mg composite. In contrary the Ti/54/91 composite, which showed the highest mechanical properties in this work, also displays Mg_2Si in its XRD spectra. Therefore it is unclear if the Mg_2Si in the Ti_3SiC_2/Mg composite plays an enhancing or detrimental role in regards to mechanical

properties. It has, however, been concluded that Mg_2Si does indeed exist in between the Ti_3SiC_2 reinforcement particles as confirmed by energy dispersive spectroscopy (Fig. 42). The existence of Mg_2Si needs to be further confirmed by surveying more areas of the Ti_3SiC_2/Mg and Ti_3SiC_2/Mg-alloy composites in order to develop a solid foundation in understanding how prevalent its volume fraction is in the composite microstructure.

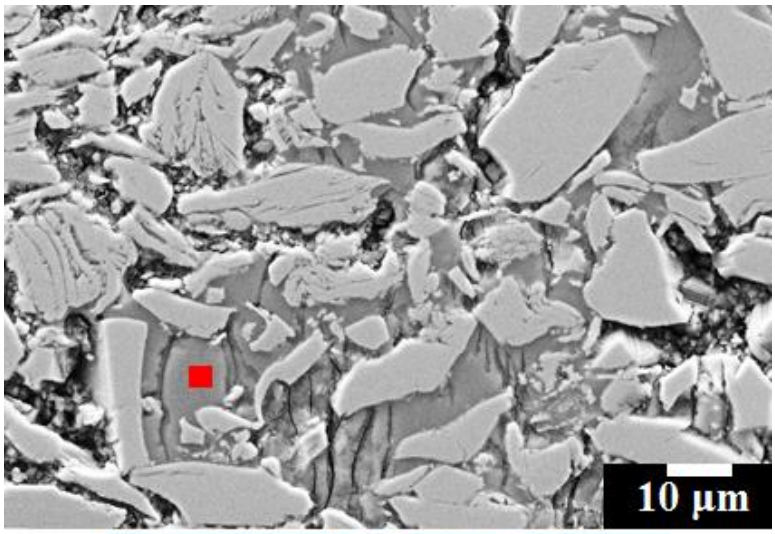

Element	Mg	Si	C
Atomic %	56.6	29.2	14.2

Figure 42: SEM image displaying the Ti/55/31 composite location where EDS has revealed the appropriate atomic % ratio consistent with Mg_2Si.

9. Other Work Aspects

9.1 Safety

This work concerned itself with several aspects requiring safety considerations. In general, the safety requirements to satisfy this work were always considered with strict guidelines always being abided to and followed. The appropriate personal protective equipment (PPE) for each work environment was always worn. In some circumstances, the work environment demanded additional PPE.

Fine powder handling and mixing was a consistent activity in this work. Careful consideration of handling and storage of metal and MAX phase powders was practiced. Fine powders can be toxic if inhaled or ingested, and can be highly flammable or even explosive if exposed to flame, spark, or locally increased temperatures. Metal and MAX phase powders were stored in a flammable cabinet. A dust mask, gloves, safety glasses and lab coat were always worn when working with metal or MAX phase powders. In the case of milling MAX phase bricks at the Drexel Machine shop, a half-face respirator with the appropriate filtration cartridges was worn in addition to the required PPE.

The vacuum hot press has high operating temperature (1600^{o}C) capability and uses electronically controlled hydraulics capable of pressing to 100 tons. The hot press runs on low voltage and high amperage making it a potential deadly hazard. Taking the necessary precautions to work in this environment was always practiced. Gloves, a lab coat and safety glasses were always worn in this environment.

Instron mechanical testing equipment was used to gather all necessary data for the analysis in this work. The Instron testing environment can cause serious injuries if it is not respected. It is a heavy equipment environment with pinch points and the possibility of shattered debris. Injuries such as crushed fingers or limbs can be the result of inappropriate safety considerations. The proper PPE was always worn in this testing environment. A thick plastic shield was always placed in front of the equipment during testing to negate any sample shattering effects.

9.2 SOPS

All standard operating procedures and instructional training videos can be found through accessing the password protected MAX Phase and MXene Research Group website at http://max.materials.drexel.edu/.

9.3 MSDS

A complete list of MSDS for materials used in this work can be found can be found through accessing the password protected MAX Phase and MXene Research Group website at http://max.materials.drexel.edu/.

9.4 Standards

It has been reported previously in this work that the linear intercept method as described by ASTM E112-10 was used for grain size analysis. Unique, specifically designed ultimate compression and cyclic compression tests for this work have no documented standard. However, there are similar standards for testing composites such as the ASTM C1358 series of standards. Although these standards can be observed as

similar, using them would not be sufficient to replicate the work herein. However, ASTM E 9, “Compression testing of Metallic Materials at Room Temperature”, DIN 50106, “Compression Test, Testing of Metallic Materials” and ASTM E 209, “Compression Tests of Metallic Materials at Elevated Temperatures with Conventional or Rapid Heating Rates and Strain Rates” may prove to be relatable in physics and mode of operation.[45]

9.5 Budget

A budget was constructed on the basis of the amount of engineering labor hours or stipend, materials, hardware and software usage for synthesis and fabrication of these composites, characterization tool usage time and subscriptions (if any), laboratory hardware maintenance or repair and machining outsourcing costs (Fig. 43).

Charge	Expense
Metallographic Materials	200
Powders	1000
Metals and Alloys	1600
Machining	4000
Gases	200
Characterization & Testing	2000
Hardware Main/Repair	4000
Salary	12600
Total	**25600**

Figure 43: Charge types and their related costs.

9.6 Ethics

No studies on toxicity were performed on the materials in this work. It is however to be assumed that Cr_2AlC may have toxic or carcinogenic effects as chromium is already considered carcinogenic and a hazard to human health. The final composite products synthesized in this work have no odor, leave no residue behind and are completely stable at ambient conditions.

These composites, which show improved mechanical properties to that of the AZ alloys used as their matrices, may offer a better safety figure of merit for applications in aircraft and automotive industries. This is one of the positive outcomes of creating these materials: envisioning their usage one day in important applications for society's use.

The current processing techniques to create these composites have a very low environmental impact: waste is on a low scale and any waste products have a good possibility to be recycled and reused again or used for other applications. The energy consumption of vacuum hot pressing of such small scale materials, however, is not a sustainable process for industrial use. A more effective and efficient one-step processing method would need to be developed in order to industrialize these materials for use.

9.7 Time Management

A careful assessment of time management was necessary in order to complete a quality thesis successfully. A Gantt chart was created early in the fall quarter of the 2013-2014 academic year to provide target dates, give clarity on progress and ultimately stay on schedule for graduation (Fig 44).

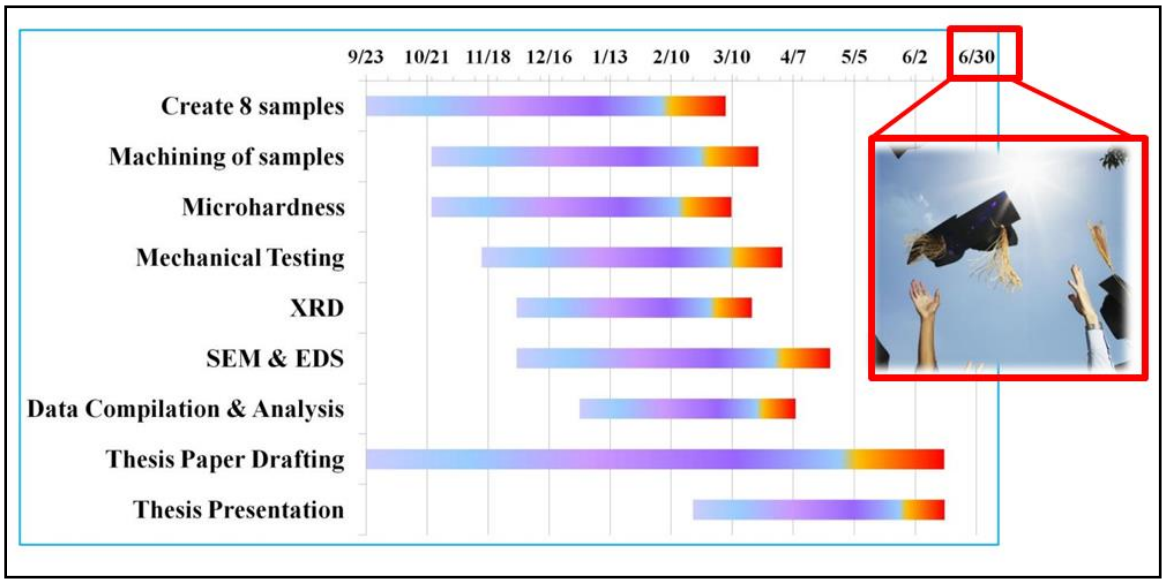

Figure 44: Gantt chart displaying time management schedule for the successful completion of this work.

List of References

1 Fridell, J. *Military Technology*. 20-25 (Lerner Publications Co., 2008).

2 Gupta, M. & Sharon, N. M. L. 277 (Wiley, Honoken, NJ, USA, 2010).

3 Mordike, B. L. & Ebert, T. Magnesium: Properties — applications — potential. *Materials Science and Engineering: A* **302**, 37-45 (2001).

4 Barrena, M. I., de Salazar, J. M. G., Matesanz, L. & Soria, A. Effect of heat treatments on oxidation kinetics in AZ91 and AM60 magnesium alloys. *Materials Characterization* **62**, 982-986, doi:10.1016/j.matchar.2011.07.001 (2011).

5 Friedrich, H. & Schumann, S. Research for a "new age of magnesium" in the automotive industry. *Journal of Materials Processing Technology* **117**, 276-281 (2001).

6 Furuya, H., Kogiso, N., Matunaga, S. & Senda, K. Applications of Magnesium Alloys for Aerospace Structure Systems. *Trans Tech Publ*, 341-348 (2000).

7 (ed Number of scientific articles which have terms AZ91 or AZ31 in the abstract) (Cambridge Scientific Abstracts Database, 2009).

8 Miracle, D. B. & Donaldson, S. L. in *ASM Handbook* Vol. 21 3-17 (ASM International, 2001).

9 Rawal, S. Metal-matrix composites for space applications. *Jom-Journal of the Minerals Metals & Materials Society* **53**, 14-17, doi:10.1007/s11837-001-0139-z (2001).

10 Ye, H. & Liu, X. Review of recent studies in magnesium matrix composites. *Journal of Materials Science* **39**, 6153-6171, doi:10.1023/b:jmsc.0000043583.47148.31 (2004).

11 Thakur, S. K., Srivatsan, T. S. & Gupta, M. Synthesis and mechanical behavior of carbon nanotube-magnesium composites hybridized with nanoparticles of alumina. *Materials Science and Engineering a-Structural Materials Properties Microstructure and Processing* **466**, 32-37, doi:10.1016/j.msea.2007.02.122 (2007).

12 Yoo, S. J., Han, S. H. & Kim, W. J. Magnesium matrix composites fabricated by using accumulative roll bonding of magnesium sheets coated with carbon-nanotube-containing aluminum powders. *Scripta Materialia* **67**, 129-132, doi:10.1016/j.scriptamat.2012.03.040 (2012).

13 Babu, J. S. S., Nair, K. P., Unnikrishnan, G., Kang, C. G. & Kim, H. H. Fabrication and Properties of Magnesium (AM50)-based Hybrid Composites with Graphite Nanofiber and Alumina Short Fiber. *Journal of Composite Materials* **44**, 971-987, doi:10.1177/0021998309349548 (2010).

14 Chawla, N. & Chawla, K. K. (Spring Science+Business Media, Inc., New York, NY, 2006).

15 Kevorkijan, V. Mg AZ80/SiC composite bars fabricated by infiltration of porous ceramic preforms. *Metallurgical and Materials Transactions a-Physical Metallurgy and Materials Science* **35A**, 707-715, doi:10.1007/s11661-004-0381-4 (2004).

16 Wang, H. Y., Jiang, Q. C., Wang, Y., Ma, B. X. & Zhao, F. Fabrication of TiB2 particulate reinforced magnesium matrix composites by powder metallurgy. *Materials Letters* **58**, 3509-3513, doi:http://dx.doi.org/10.1016/j.matlet.2004.04.038 (2004).

17 Information, G. A. P. C. O. n. *GE Aviation selects Indiana for $100 million jet engine assembly factory*, <http://www.geaviation.com/press/other/other_20140326.html> (2014).

18 Lloyd, D. J. Partilce reinforced aluminum magnesium matrix composites. *International Materials Reviews* **39**, 1-23 (1994).

19 Reddy, S. U., Srikanth, N., Gupta, M. & Sinha, S. K. Enhancing the properties of magnesium using SiC particulates in sub-micron length scale. *Advanced Engineering Materials* **6**, 957-964 (2004).

20 Ugandhar, S., Gupta, M. & Sinha, S. K. Enhancing strength and ductility of Mg/SiC composites using recrystallization heat treatment. *Composite Structures* **72**, 266-272, doi:http://dx.doi.org/10.1016/j.compstruct.2004.11.010 (2006).

21 Saravanan, R. A. & Surappa, M. K. Fabrication and characterisation of pure magnesium-30 vol.% SiCP particle composite. *Materials Science and Engineering: A* **276**, 108-116, doi:http://dx.doi.org/10.1016/S0921-5093(99)00498-0 (2000).

22 Gupta, M., Lai, M. O. & Saravanaranganathan, D. Synthesis, microstructure and properties characterization of disintegrated melt deposited Mg/SiC composites. *Journal of Materials Science* **35**, 2155-2165 (2000).

23 Contreras, A., López, V. H. & Bedolla, E. Mg/TiC composites manufactured by pressureless melt infiltration. *Scripta Materialia* **51**, 249-253, doi:http://dx.doi.org/10.1016/j.scriptamat.2004.04.007 (2004).

24 Contreras, A., Leon, C. A., Drew, R. A. L. & Bedolla, E. Wettability and spreading kinetics of Al and Mg on TiC. *Scripta Materialia* **48**, 1625-1630, doi:10.1016/s1359-6462(03)00137-4 (2003).

25 Osetzky, D. Macrocrystalline Graphite From Magnesium Carbide. *Carbon* **12**, 517-523 (1974).

26 Anasori, B., Caspi, N. & Barsoum, M. W. Fabrication and Mechanical Properties of Pressureless Melt Infiltrated Magnesium Alloy Composites Reinforced with TiC and Ti2AlC Particles. *Submitted for publication* (2014).

27 Wang, J.-j., Guo, J.-h. & Chen, L.-q. TiC/AZ91D composites fabricated by in situ reactive infiltration process and its tensile deformation. *Transactions of Nonferrous Metals Society of China* **16**, 892-896, doi:http://dx.doi.org/10.1016/S1003-6326(06)60346-4 (2006).

28 Cao, W., Zhang, C. F., Fan, T. X. & Zhang, D. In Situ Synthesis and Compressive Deformation Behaviors of TiC Reinforced Magnesium Matrix Composites. *Materials Transactions* **49**, 2686-2697, doi:10.2320/matertrans.MRA2008157 (2008).

29 Chen, L. Q., Dong, Q., Zhao, M. J., Bi, J. & Kanetake, N. Synthesis of TiC/Mg composites with interpenetrating networks by in situ reactive infiltration process. *Materials Science and Engineering a-Structural Materials Properties Microstructure and Processing* **408**, 125-130, doi:10.1016/j.msea.2005.07.036 (2005).

30 Barsoum, M. W. *MAX Phases: Properties of Machinable Ternary Carbides and Nitrides*. 436 (Wiley-VCH, 2013).

31 Liu, Z., Waki, T., Tabata, Y. & Nakamura, H. Mn-doping-induced itinerant-electron ferromagnetism in Cr2GeC. *Physical Review B* **89**, doi:10.1103/PhysRevB.89.054435 (2014).

32 Ingason, A. S. *et al.* A Nanolaminated Magnetic Phase: Mn2GaC. *Materials Research Letters* **2**, 89-93, doi:10.1080/21663831.2013.865105 (2013).

33 Anasori, B. *Table of the known $M_{n+1}AX_{n\ phases}$*, <http://max.materials.drexel.edu/research-areas/max-phases/> (2013).

34 Barsoum, M. W. & El-Raghy, T. The MAX phases: Unique new carbide and nitride materials - Ternary ceramics turn out to be surprisingly soft and machinable, yet also heat-tolerant, strong and lightweight. *American Scientist* **89**, 334-343, doi:10.1511/2001.28.736 (2001).

35 Barsoum, M. W., Zhen, T., Kalidindi, S. R., Radovic, M. & Murugaiah, A. Fully reversible, dislocation-based compressive deformation of Ti3SiC2 to 1GPa. *Nature Materials* **2**, 107-111, doi:10.1038/nmat814 (2003).

36 Zhou, A. G. & Barsoum, M. W. Kinking nonlinear elastic deformation of Ti3AlC2, Ti2AlC, Ti3Al(C-0.5,N-0.5)(2) and Ti2Al(C-0.5,N-0.5). *Journal of Alloys and Compounds* **498**, 62-70, doi:10.1016/j.jallcom.2010.03.099 (2010).

37 Amini, S., Ni, C. & Barsoum, M. W. Processing, microstructural characterization and mechanical properties of a Ti2AlC/nanocrystalline Mg-matrix composite. *Composites Science and Technology* **69**, 414-420, doi:http://dx.doi.org/10.1016/j.compscitech.2008.11.007 (2009).

38 Amini, S. *et al.* On the Stability of Mg Nanograins to Coarsening after Repeated Melting. *Nano Letters* **9**, 3082-3086, doi:10.1021/nl9015683 (2009).

39 Barsoum, M. W. & El-Raghy, T. Synthesis and Characterization of a Remarkable Ceramic: Ti3SiC2. *Journal of the American Ceramic Society* **79**, 1953-1956, doi:10.1111/j.1151-2916.1996.tb08018.x (1996).

40 Zhou, W. B., Mei, B. C. & Zhu, J. Q. On the synthesis and properties of bulk ternary Cr2AlC ceramics. *Materials Science-Poland* **27**, 973-980 (2009).

41 *Alloy Data: Magnesium Alloys*, <http://www.tcdcinc.com/media/2009_NADCA_Alloy_Data.pdf> (2009).

42 Barsoum, M. W. & Basu, S. in *Encyclopedia of Materials: Science and Technology* (eds K.H.J. Buschow *et al.*) 1-23 (Elsevier, Oxford, 2010).

43 Staff, M. E. *RSMeans Illustrated Construction Dictionary*. (John Wiley & Sons, 2012).

44 Housh, S., Mikucki, B. & Stevenson, A. in *ASM* Vol. 2 Ch. Selection and Application of Magnesium and Magnesium Alloys, (ASM International, 2005).

45 Kuhn, H. A. *Uniaxial Compression Testing*. Vol. 8 (ASM International, 2005).